[redacted] EC Category: HEALTH AND SAFETY

CEX-62.81 (Prelim.)

CIVIL EFFECTS STUDY

GROUND ROUGHNESS EFFECTS ON THE ENERGY AND ANGULAR DISTRIBUTION OF GAMMA RADIATION FROM FALLOUT

C. M. Huddleston, Z. G. Burson,
R. M. Kinkaid, and Q. G. Klingler

Issuance Date: May 22, 1963

CIVIL EFFECTS TEST OPERATIONS
U.S. ATOMIC ENERGY COMMISSION

NOTICE

This report is published in the interest of providing information which may prove of value to the reader in his study of effects data derived principally from nuclear weapons tests and from experiments designed to duplicate various characteristics of nuclear weapons.

This document is based on information available at the time of preparation which may have subsequently been expanded and re-evaluated. Also, in preparing this report for publication, some classified material may have been removed. Users are cautioned to avoid interpretations and conclusions based on unknown or incomplete data.

PRINTED IN USA
Price $1.25. Available from the Office of Technical Services, Department of Commerce, Washington 25, D. C.

USAEC Division of Technical Information Extension, Oak Ridge, Tennessee

GROUND ROUGHNESS EFFECTS ON THE ENERGY AND ANGULAR DISTRIBUTION OF GAMMA RADIATION FROM FALLOUT

By

C. M. Huddleston
(U. S. Naval Civil Engineering Laboratory,
Port Hueneme, California)
Z. G. Burson
R. M. Kinkaid
Q. G. Klingler

Approved by: L. J. DEAL
Acting Chief
Civil Effects Branch

Edgerton, Germeshausen & Grier, Inc.
Las Vegas, Nevada
November 1962

ACKNOWLEDGMENTS

The authors wish to express their appreciation to L. J. Deal, Acting Chief, Civil Effects Branch, Division of Biology and Medicine, U. S. Atomic Energy Commission; his personal initiative and continued support made this project possible. The authors are also indebted to John Auxier of Oak Ridge National Laboratory, who suggested the need for this investigation, for the many useful ideas he contributed to the planning of the experiment.

Appreciation is expressed to the U. S. Naval Civil Engineering Laboratory, Port Hueneme, Calif., for lending the truck used in the field operations.

Valuable assistance was received from W. G. Markland and P. C. Murphy in the operational phases of the experiment.

W. E. Page made important contributions to the reduction of the data.

CONTENTS

ILLUSTRATIONS

ILLUSTRATIONS Continued

CHAPTER 3 EXPERIMENTAL ARRANGEMENT

CHAPTER 4 FIELD OPERATIONS

CHAPTER 5 RESULTS

APPENDIX B METHOD FOR DETERMINING APPROXIMATE DOSE FROM SPECTRUM MEASUREMENTS

TABLE

APPENDIX A PREDICTION OF FALLOUT CONTOURS

Chapter 1

INTRODUCTION

The importance of ground roughness as a mechanism for natural shielding from fallout radiation has long been recognized,[1] and experimental measurements have been made of dose vs. height above a rough plane. In the theoretical treatment of ground-roughness shielding, it has been generally supposed that radioactivity could be considered as being mixed uniformly with soil throughout a surface layer of a smooth plane, the depth of the surface layer depending on the degree of ground roughness.

Alternatively, a simpler model can be used where the fallout is treated as though it were buried beneath the surface of an infinite smooth plane, the depth of the hypothetical fallout layer depending on the roughness of the ground.[1–3] This simpler model is clearly to be preferred if it gives satisfactory agreement with experiment because the calculations to be performed are easier.

An earlier investigation[3] was concerned with the measurement of the angular distribution and energy distribution of fallout radiation above a nearly level desert pavement of coarse gravel that was relatively free of sagebrush. Dose-vs.-height measurements were not made as a part of that investigation.

In another experiment[4] the angular distribution of dose was determined 1 m above ground that had been contaminated with Cs^{137}. In both the experimental determinations of the angular distribution of dose, it was found that the dose was maximum in a direction almost parallel to the surface of the contaminated ground.

In any determination of the importance of ground roughness as a factor in shielding, it is important to ascertain the angular distribution of dose and the variation of dose with height above types of terrain with varying degrees of roughness. It is also valuable in shielding calculations to know the energy spectrum of the gamma radiation. The investigation reported here was directed toward resolving these problems.

REFERENCES

1. C. F. Ksanda, A. Moskin, and E. S. Shapiro, *Gamma Radiations from a Rough Infinite Plane*, USAEC Report USNRDL-TR-108, U. S. Naval Radiological Defense Laboratory, Jan. 18, 1956.
2. L. V. Spencer, Structure Shielding Against Fallout Radiation from Nuclear Weapons, *Natl. Bur. Std. (U. S.) Monograph, No. 42* (1962).
3. R. L. Mather, R. F. Johnson, F. M. Tomnovec, and C. S. Cook, *Gamma Radiation Field Above Fallout Contaminated Ground*, Operation Teapot Report, WT-1225, U. S. Naval Radiological Defense Laboratory, Oct. 28, 1959.
4. C. E. Clifford, J. A. Carruthers, and J. R. Cunningham, Gamma Radiation at Air-Ground Interfaces with Distributed Cs^{137} Sources, *Can. J. Phys.*, 38: 504 (1960). Also see, C. E. Clifford, J. A. Carruthers, and J. R. Cunningham, *Scattered Radiation from a Simulated Fallout Field Using Cs^{137}*, Report No. 296, Defence Research Board of Canada, Defence Research Chemical Laboratories, Ottawa, January 1959.

Chapter 2

THEORY OF THE EXPERIMENT

2.1 DESCRIPTION OF THE ACTUAL PROBLEM

In the case where actual fallout is nonuniformly distributed over irregular terrain, a calculation of the energy and angular distributions of radiation incident at some point above the ground is exceedingly complicated. Factors entering into the calculations would include (1) the shape of the ground surface within approximately two mean free paths of the detector, (2) the surface distribution of fallout, and (3) the energy distribution of gamma radiation emitted by fallout.

Even if it were possible to perform a detailed calculation involving microscopic surface features allowing for the possibility that the fallout might be nonuniformly mixed with varying amounts of topsoil, for variation in the gamma-ray spectrum of fallout radiation with time, and for the fact that not all fallout particles have the same gamma-ray emission spectrum, it is highly doubtful that such a calculation would be worthwhile. A detailed calculation of this type would probably be prohibitively difficult, and results obtained would apply only for the specific cases treated.

On the other hand, it may be possible to make some simplifying assumptions and approximations so that the problem can be handled with relative ease and, at the same time, theoretical results can be obtained which bear sufficient resemblance to reality to be interesting and useful.

2.2 INFINITE-PLANE SOURCE

Begin with a treatment of an infinite-plane isotropic source of monochromatic radiation in air and compute the directly incident radiation.

The quantities r, h, and θ are as shown in the adjacent figure. It is seen that

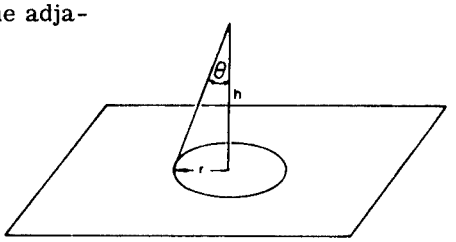

$$dI = \frac{2\pi r S e^{-\alpha/\cos\theta}}{4\pi\,(h/\cos\theta)^2}\,dr$$

where I = radiation intensity at the detector in photons per second per steradian
S = source strength in photons per square centimeter per second
α = number of mean free paths of air between the source and the detector

If Ω is a solid angle,

$$d\Omega = 2\pi \sin\theta\, d\theta$$

and

$$r = h \tan \theta$$

$$dr = h \sec^2 \theta \, d\theta$$

Thus

$$\frac{dI}{d\Omega} = \frac{Se^{-\alpha/\cos\theta}}{4\pi \cos \theta} \tag{2.1}$$

It should be evident that Eq. 2.1 is valid if the source is deposited in an infinite plane below a smooth infinite surface of earth, providing it is understood that α refers to the number of mean free paths of matter between the source and the detector.

2.3* APPROXIMATE TREATMENT OF EFFECTS OF GROUND ROUGHNESS

The case where the terrain is irregular can be treated by the approximation that the actual case is represented by an infinite-plane source buried some distance below a smooth infinite surface of earth.[1] A family of curves showing the relation between $I(\theta)$ and $\cos \theta$ for various values of α is plotted in Fig. 2.1.

An interesting relation can now be derived between α and the angle for which the radiation intensity is a maximum. Differentiating Eq. 2.1 with respect to θ,

$$\frac{\partial}{\partial\theta}\left(\frac{Se^{-\alpha/\cos\theta}}{4\pi \cos \theta}\right) = 0$$

$$\frac{\partial}{\partial\theta}\left(\frac{S}{4\pi} \sec \theta \, e^{-\alpha \sec \theta}\right) = 0$$

For $\theta > 0$,

$$\cos \theta_{max.} = \alpha \tag{2.2}$$

This simple result shows that the cosine of the angle that corresponds to maximum dose is equal to the equivalent depth of the plane source in mean free paths.

2.4 ALTERNATE METHOD FOR DETERMINING EQUIVALENT DEPTH

In Sec. 2.3 it was shown that α was a measure of ground roughness, in the sense that α measures the equivalent number of mean free paths of scattering and absorbing material between the source and the detector. In this section alternate methods for determining α are investigated. More properly an attempt is made to determine τ, which is the number of feet of air equivalent that should be attributed to ground roughness effects.[1] The relation between α and τ is that one mean free path is equivalent to approximately 500 ft of air (at 20°C, 76 cm Hg).

In the case where fallout is distributed uniformly over a smooth infinite plane, let a detector be at a distance d above the plane. The intensity of dose as a function of d and θ, where θ is the angle between the incident radiation and the normal measured down from the detector to the plane, is shown in Fig. 2.1. This graph of $l(d,\cos \theta)$ is valid for the gamma-ray spectrum of fission products 1.12 hr after the fission event. The normalization of $l(d,\cos \theta)$ is such that

$$D_0 = D(3) = \int_0^{\pi} l(3,\cos \theta) \sin \theta \, d\theta = 1$$

That is, the total dose at 3 ft above the surface is taken to be unity.

The variation of dose with height is given by

$$\frac{D}{D_0} = L(d)$$

Figure 2.2 shows how L(d) varies with d.

In the case where there is appreciable ground roughness, the variation of dose with height is less straightforward. An approximation is given by

$$\frac{D}{D_0} = L(d + \tau)$$

where τ is a parameter that gives some measure of ground roughness. The same parameter can be expected to apply for the case of angular distribution; that is, the expression

$$l(d + \tau, \cos \theta)$$

should be used to predict the angular distribution of radiation intensity at a distance d above a rough plane.

2.5 FALLOUT CONTOURS

Appendix A gives a treatment of expected fallout contours. It was necessary to make some rough predictions regarding the deposition of fallout so that appropriate areas in the vicinity of ground zero (GZ) could be thoroughly explored before D-day and so that suitable areas could be plowed in advance of the test.

REFERENCES

1. L. V. Spencer, Structure Shielding Against Fallout Radiation from Nuclear Weapons, *Natl. Bur. Std. (U. S.) Monograph, No. 42* (1962).

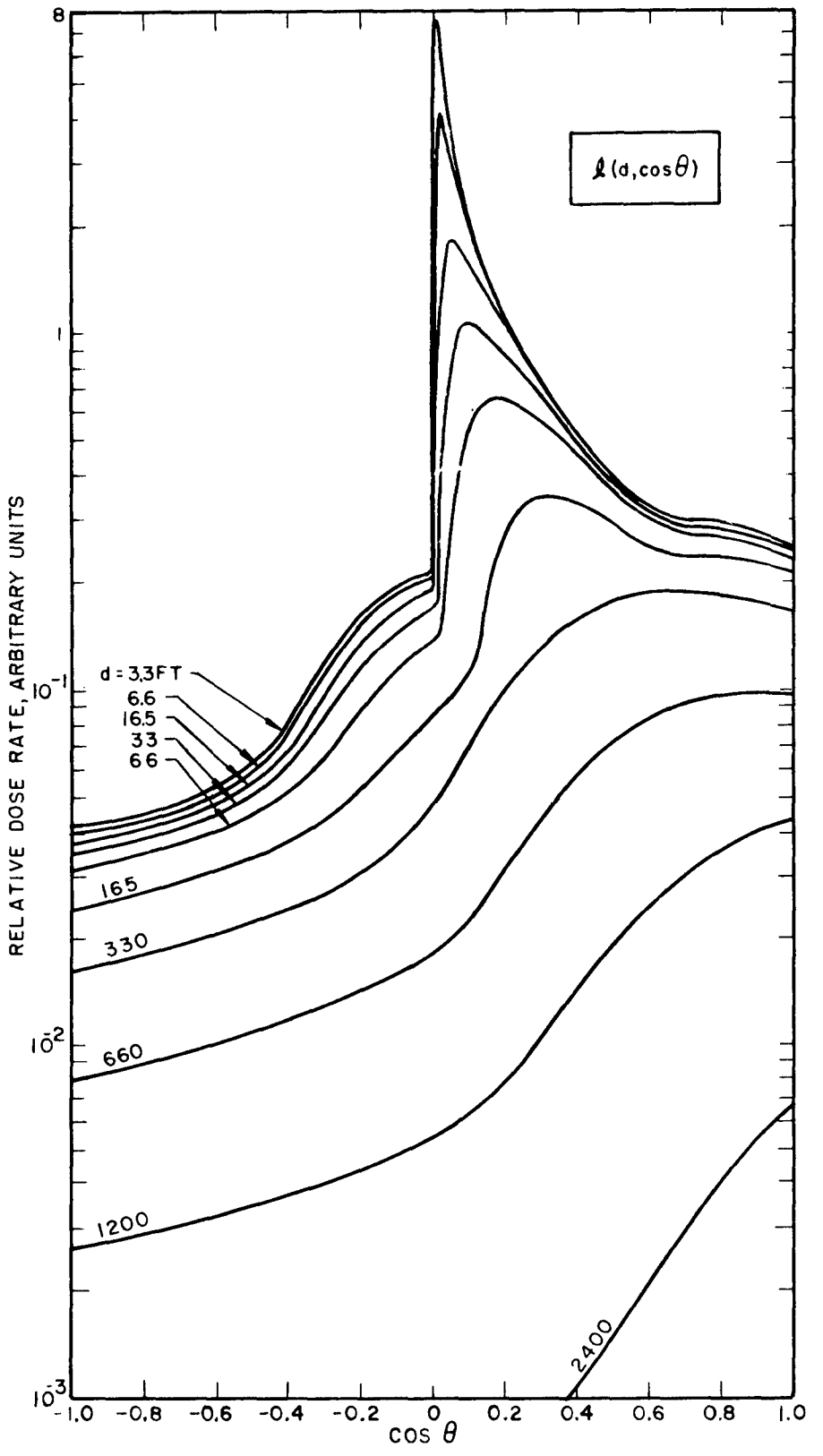

Fig. 2.1—Variation of dose with angle and height above a plane (Spencer[1]).

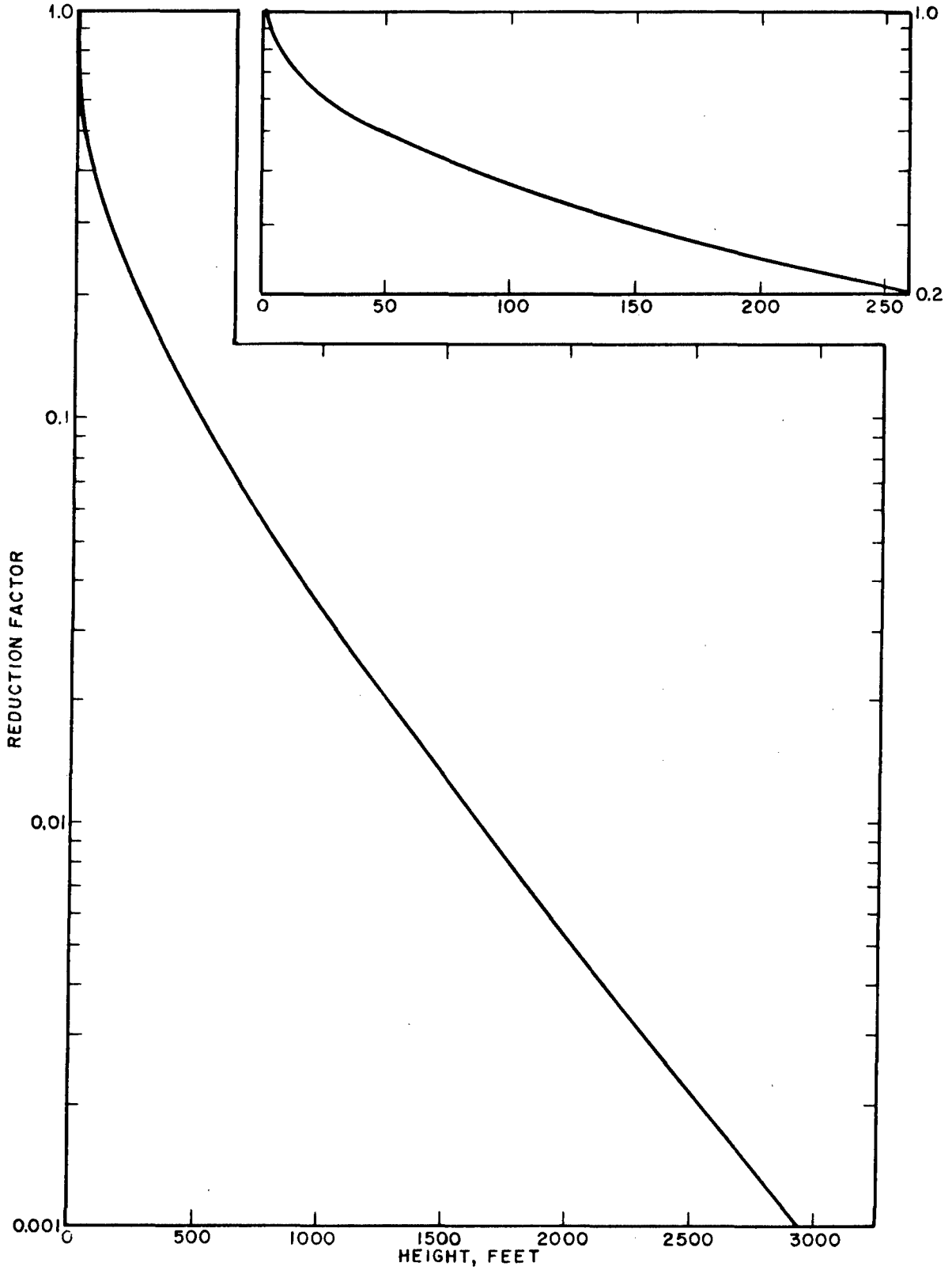

Fig. 2.2—Variation of dose with height (Spencer[1]).

Chapter 3

EXPERIMENTAL ARRANGEMENT

3.1 GAMMA-RAY DETECTOR

The principal detecting device consisted of a Harshaw integral line assembly (type 12S) with a NaI(Tl) crystal 3 in. in diameter by 3 in. high and a selected 3-in. Dumont 6363 photomultiplier tube. The resolution of the assembly was approximately 8% for the Cs^{137} 662-kev gamma-ray line.

Pulses from the phototube were fed through a 90-ft 50-ohm cable (RG-58-U) into a Nuclear Data model 130A 512-channel pulse-height analyzer. The data could be typed or recorded on punched tape.

Ionization chambers were used for local surveying and for dose-vs.-height measurements.

3.2 COLLIMATOR

The detector assembly was housed in a cylindrical lead collimator designed and built by Edgerton, Germeshausen & Grier, Inc. (EG&G), Santa Barbara, Calif. The detector was shielded on all sides by 7 in. of lead. Drawings of the collimator are shown in Figs. 3.1 and 3.2, and a photograph of the completed shield assembly appears in Fig. 3.3.

A power-driven rotating subunit allowed any of several apertures to be chosen. Figures 3.4 and 3.5 show the 0.50-in. by 20° wedge-shaped collimator aperture. There was also a 1.00-in. by 30° aperture that could be selected if the increase in counting rate justified the resultant loss in angular resolution. An insert was made to stop down the 1.00-in. by 30° aperture to a 0.50-in. cylindrical hole. Another insert provided for an aperture $\frac{1}{8}$ in. by 30°. A third position was used for calibration with an internal Cs^{137}–Co^{60} source. In the fourth position, the detector was completely shielded for background measurements.

The unorthodox wedge-shaped aperture was chosen in an attempt to improve the detector solid angle without an appreciable loss in angular resolution. This was possible because the differential dose was a sensitive function of polar angle but was not expected to be sharply dependent on azimuth. The geometry chosen (in the 0.50-in. by 20° case) allowed good resolution in polar angle (angle between the normal to the surface of the earth and the axis of the collimator aperture) and, at the same time, achieved a rather high solid angle (0.03 steradian).

The surface area of a smooth plane "seen" by the detector from a position 3 ft above the ground at various polar angles is shown in Fig. 3.6.

3.3 DOSE-VS.-HEIGHT MEASUREMENTS

Because of the importance of dose-vs.-height measurements, as mentioned in Sec. 2.4, a vertical traverse was made of dose rate as a function of height above the ground. An extension-ladder arrangement was used for this series of measurements.

3.4 MOBILE LABORATORY

A 5-ton Navy truck (borrowed from the U. S. Naval Civil Engineering Laboratory, Port Hueneme, Calif.) was modified to serve as a mobile laboratory for work in the field. Photographs of the modified six-wheel-drive truck are shown in Figs. 3.7 and 3.8. Behind the cab was an Army electrical-equipment shelter measuring approximately 7 ft by 7 ft by 11 ft long. The inside walls of the shelter were covered with a 0.5-in. thickness of lead for personnel shielding. The interior of the shielded mobile laboratory with the shock-mounted laboratory instruments and air conditioner installed is shown in Figs. 3.9 and 3.10.

Behind the shielded shelter was a wooden enclosure for housing the collimator while in transit. A 2-ton hoist was used to raise and lower the collimator.

Power for equipment, lights, and air conditioning was supplied by a 5-kva gasoline-powered motor-generator set.

Figure 3.11 shows a typical experimental setup. The collimator was operated remotely from inside the personnel shelter on the truck, which was driven at least 50 ft from the collimator location before angular distribution measurements were made.

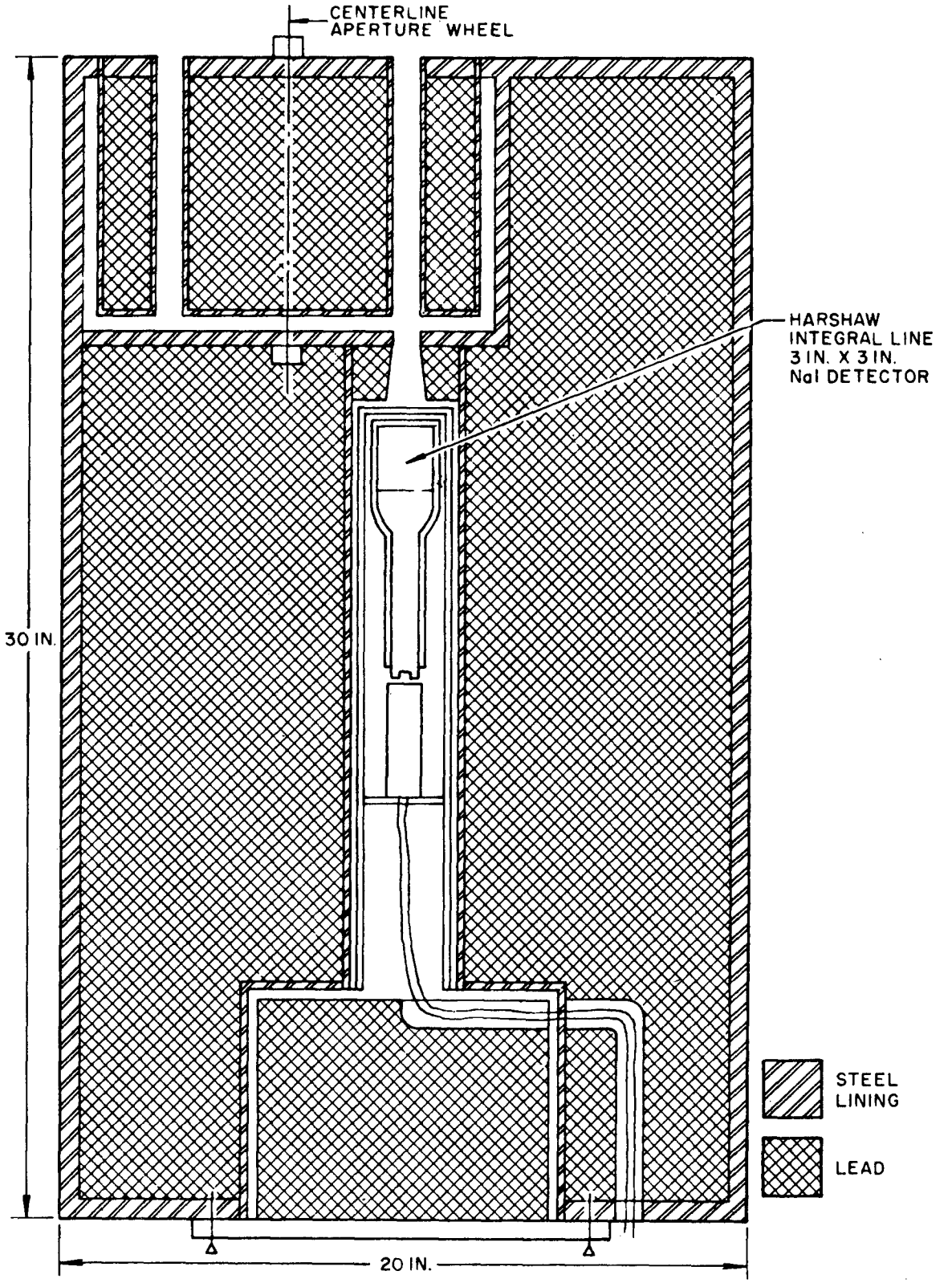

Fig. 3.1—Cross-section view of shield (not to scale).

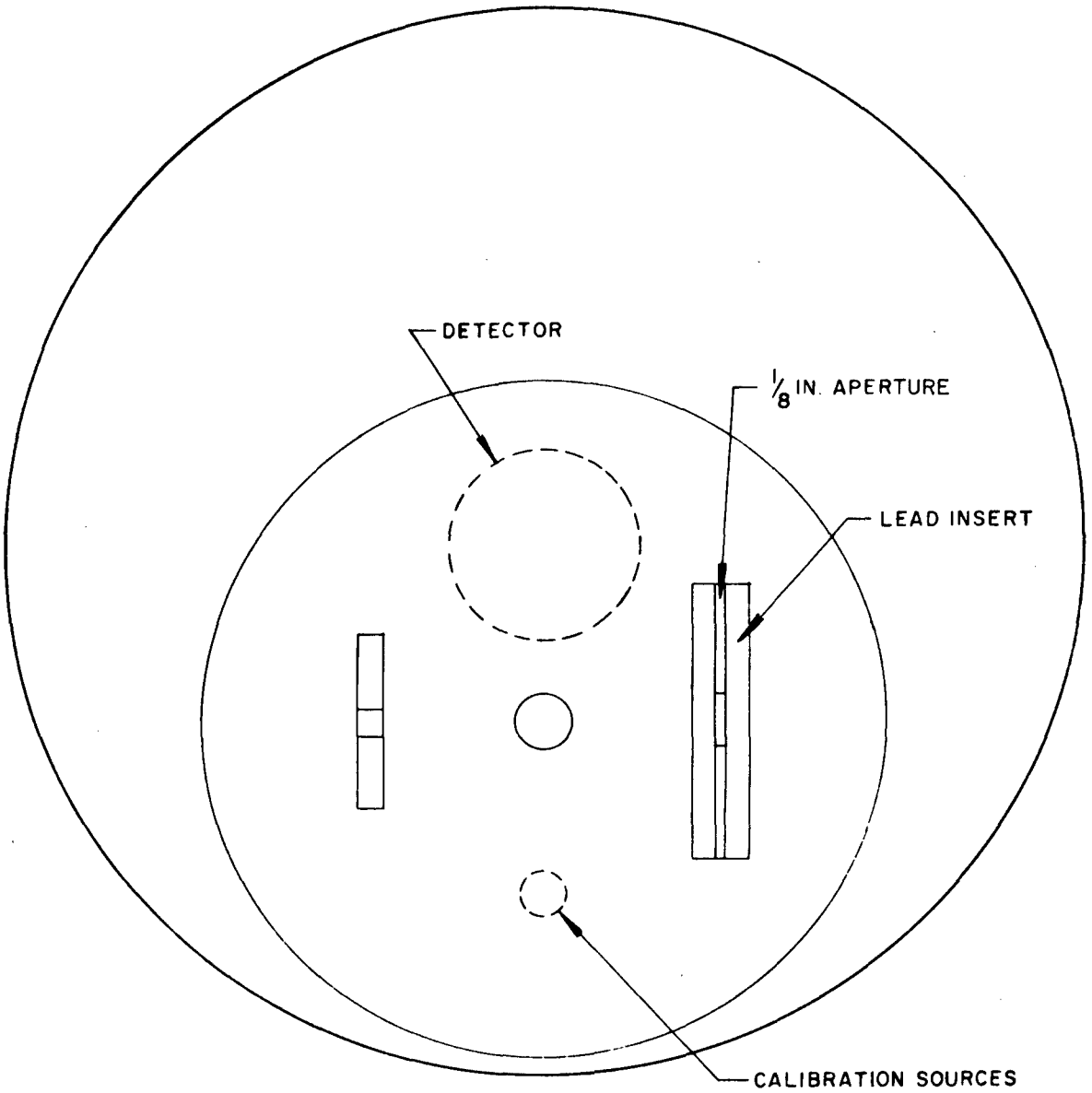

Fig. 3.2— Top view of collimator showing rotating aperture wheel in closed position.

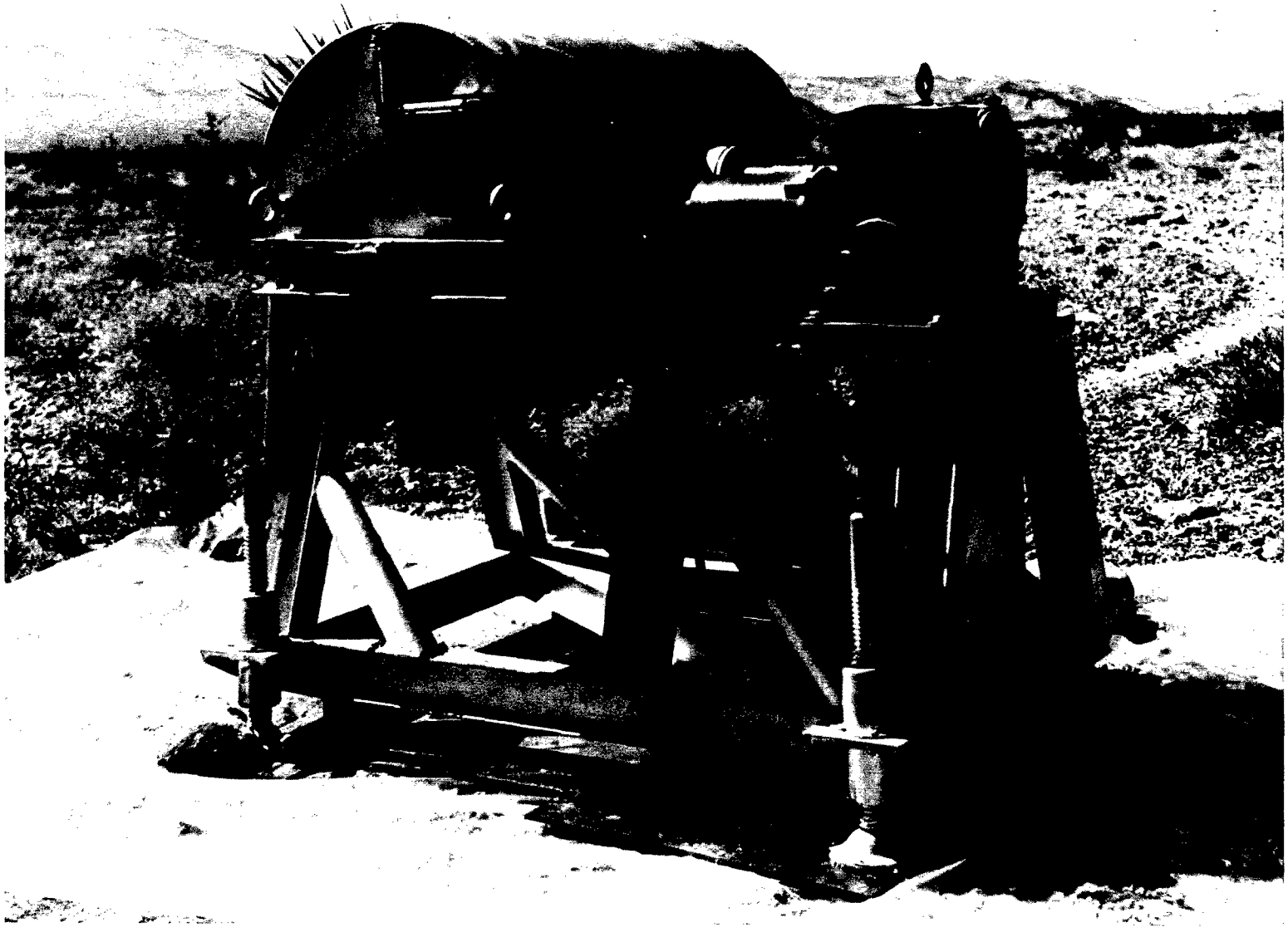

Fig. 3.3—Complete shield assembly.

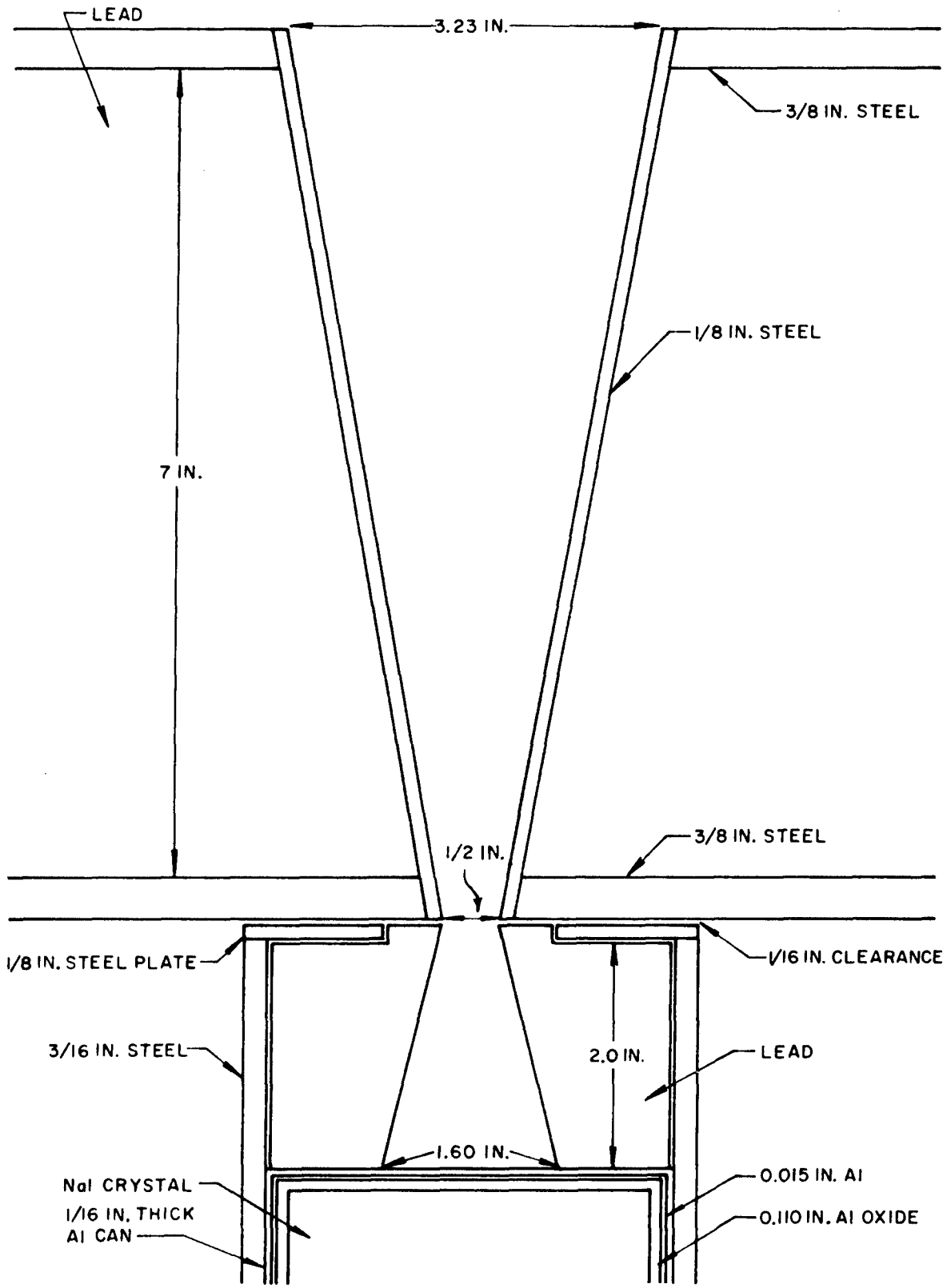

Fig. 3.4—Wedge-shaped collimator aperture, horizontal cross section.

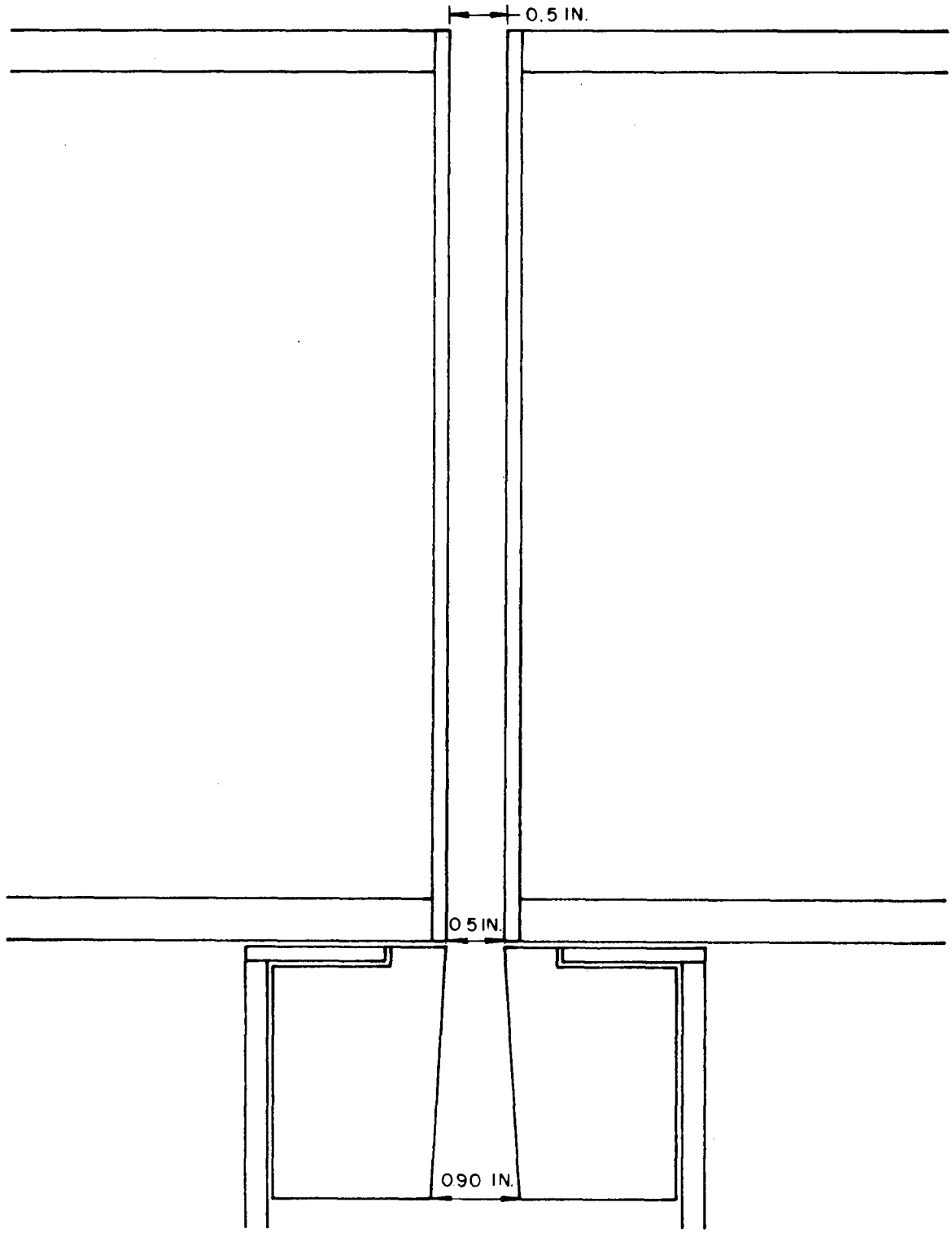

Fig. 3.5—Wedge-shaped collimator aperture, vertical cross section.

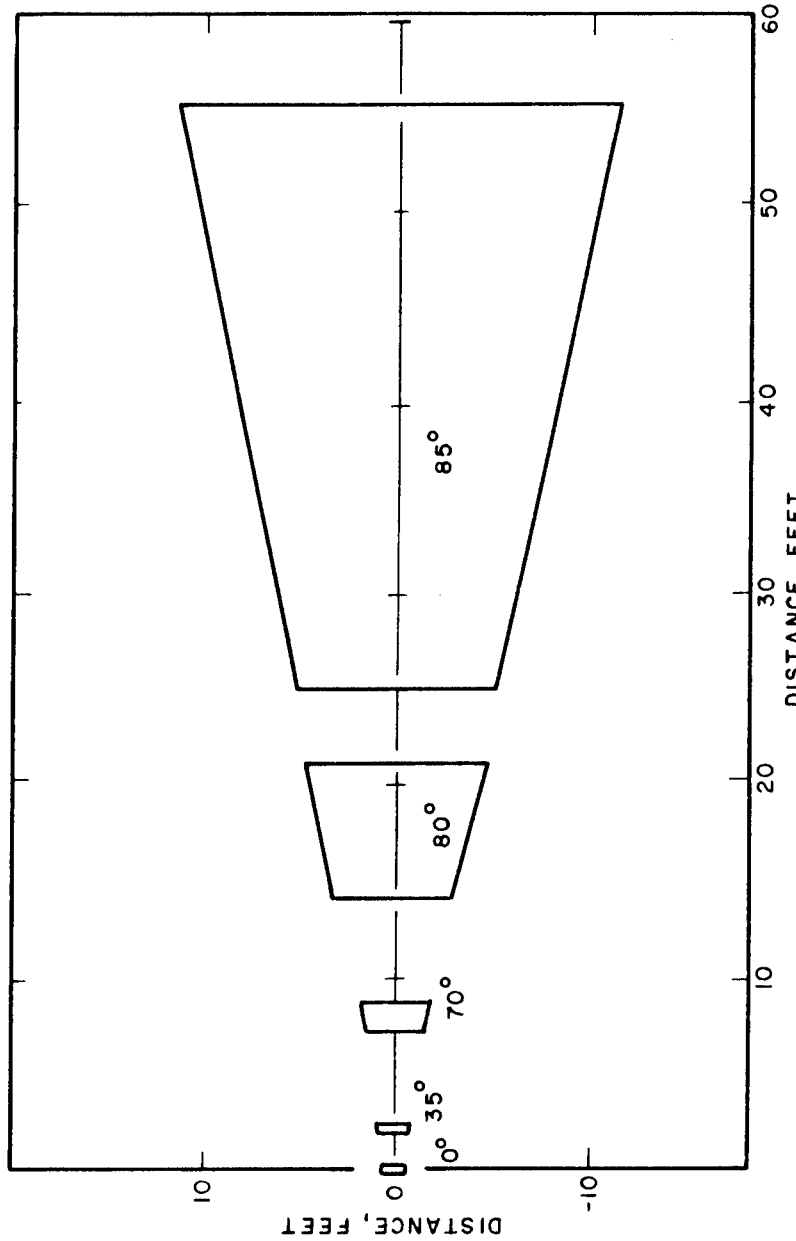

Fig. 3.6—Area seen by 0.50-in. by 20° collimator aperture as a function of polar angle.

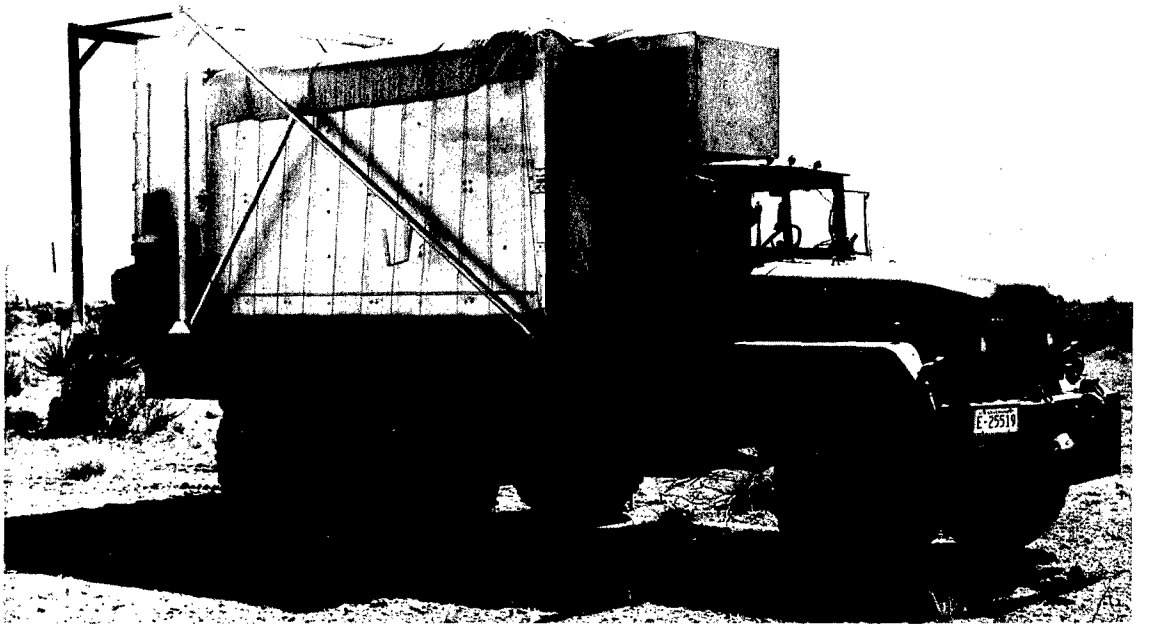

Fig. 3.7—Six wheel-drive truck.

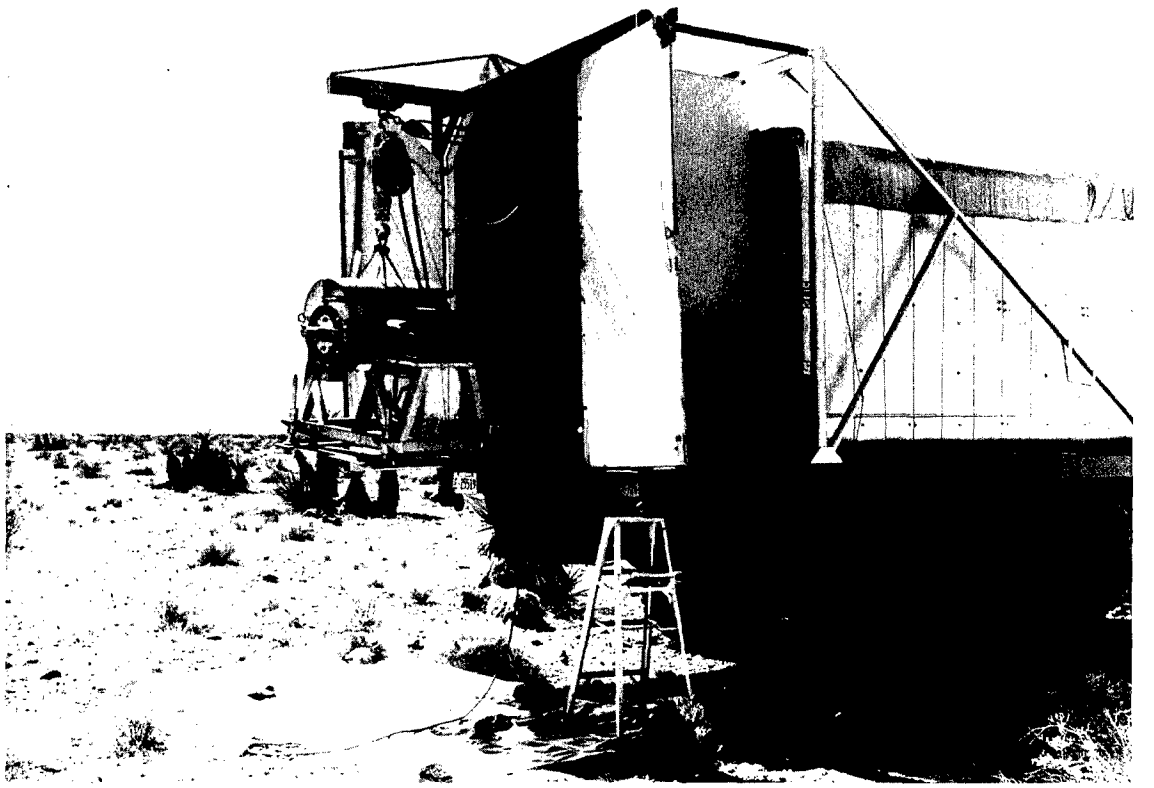

Fig. 3.8—Shield assembly on six-wheel-drive truck.

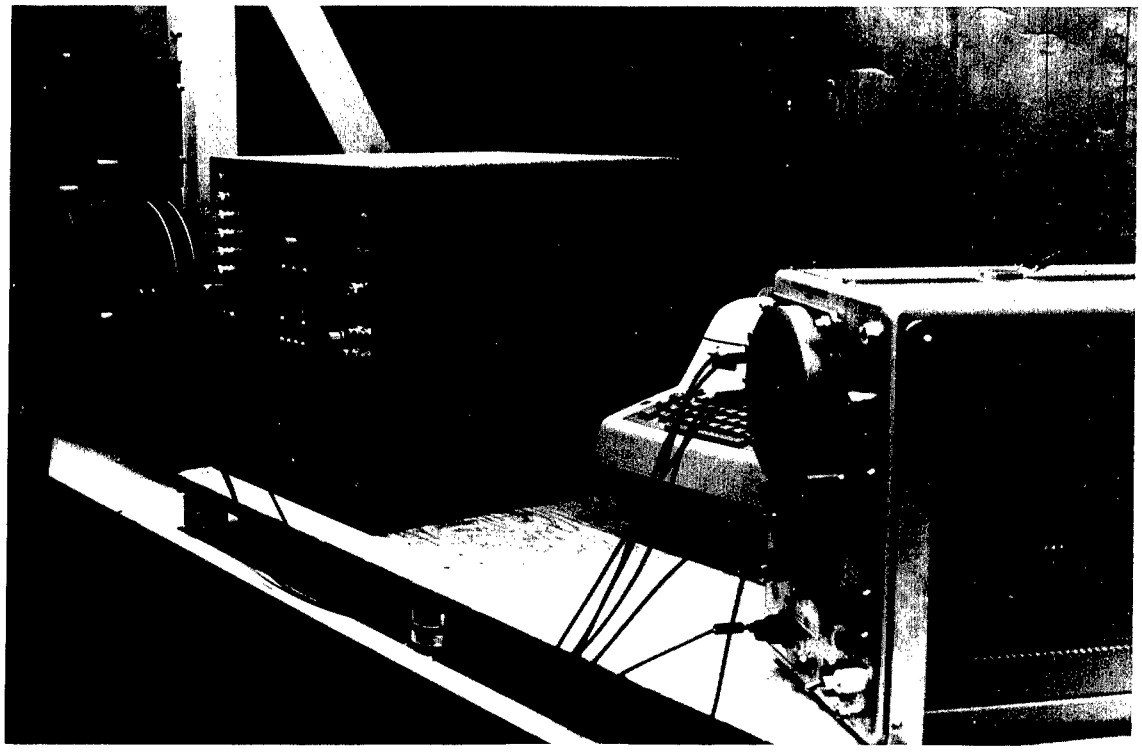

Fig. 3.9—Shock-mounted instruments, interior of shielded mobile laboratory.

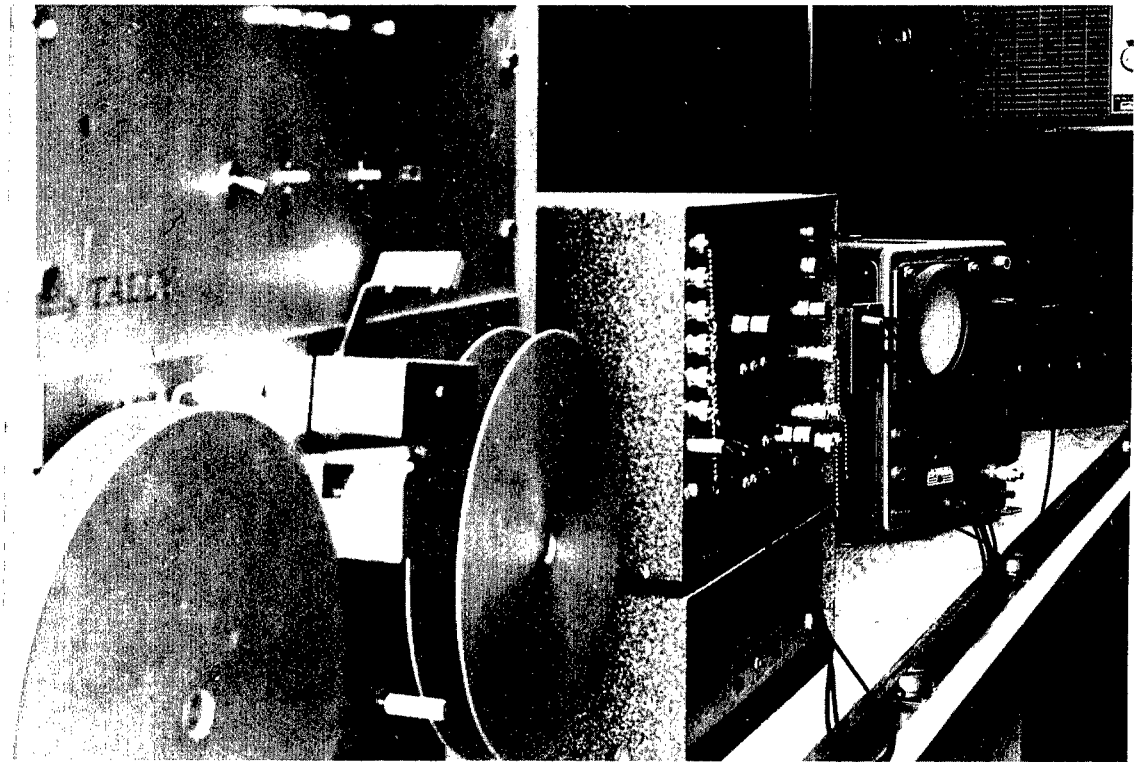

Fig. 3.10—Laboratory instruments and air conditioner, interior of shielded mobile laboratory.

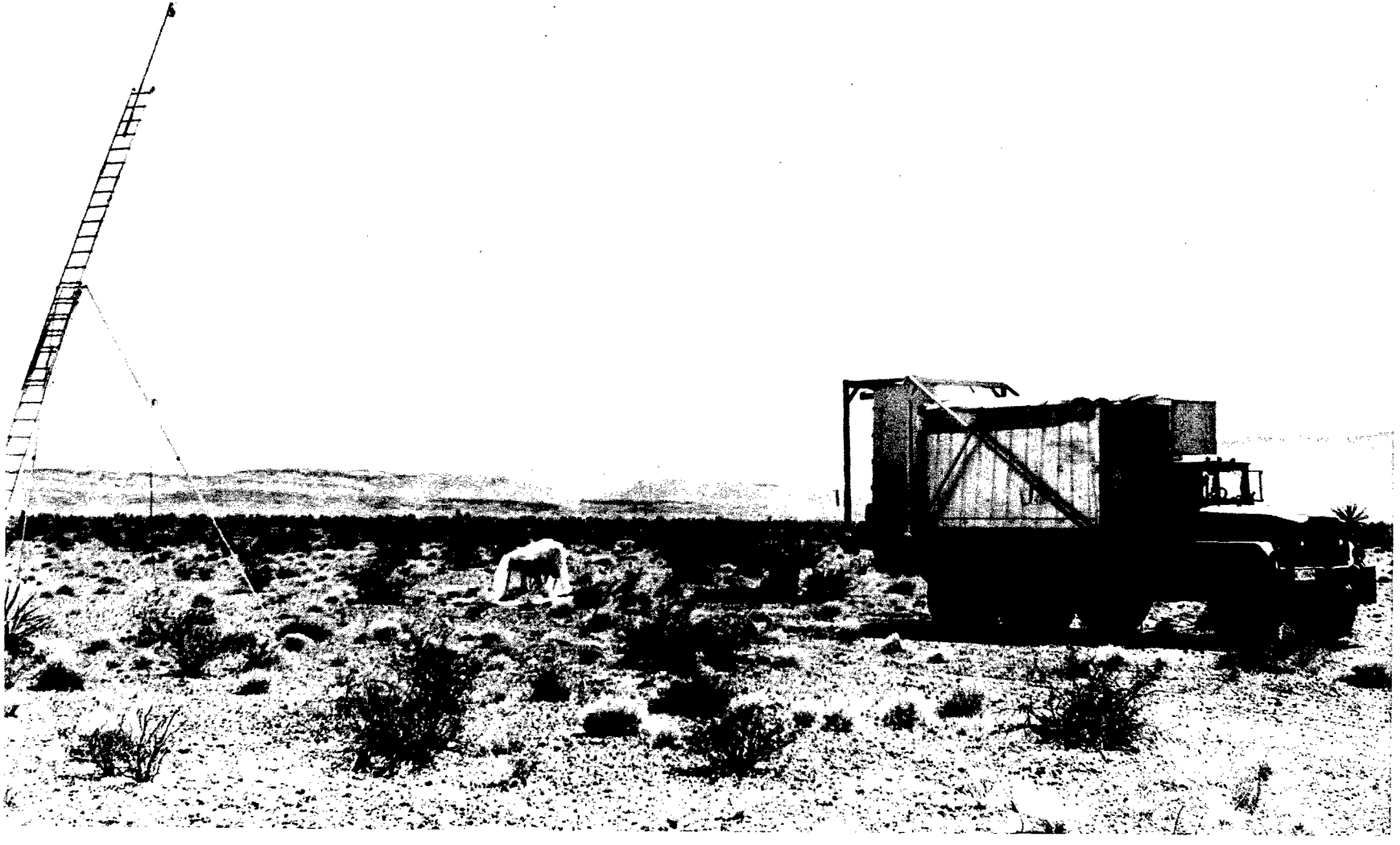

Fig. 3.11—Typical experimental setup.

Chapter 4

FIELD OPERATIONS

One type of terrain needed to meet the objectives of the project was a terrain with a known and controlled degree of roughness. Three areas were plowed several miles downwind in the predicted fallout path in the hope that fallout would be deposited on at least one. Two of these fields were located in the dry-lake bed north of Indian Springs Air Force Base, and the third, in the dry-lake bed northeast of the base. Furrows about 6 in. deep were plowed every 30 in. Each field was square and about 1500 ft on a side.

The actual fallout path was about 20° north of east from Frenchman Flat. This path missed the dry-lake beds and plowed fields in the first valley north of Indian Springs. However, the plowed field and dry-lake beds in the second valley (Range 2, about 30 miles from GZ) were near the center of the fallout pattern. The winds were rather slow, and the cloud was nearly dispersed by the time it reached the second valley. As a result, the dose rates were quite low.

Even though these dose rates were a factor of 10 lower than desirable, it was decided to obtain as much data as possible. Energy and angular-distribution measurements were made with the NaI crystal and collimator all day and evening on D + 1 day at both a dry-lake bed and at a plowed field. Long exposures were necessary to obtain valid statistical data.

Dose rate-vs.-height and decay measurements were not very successful at these two locations because of instrument problems, temperature effects, and low dose rates, even though several attempts were made on different days and nights.

Contamination appeared to be distributed quite uniformly over large areas at these two locations. Survey-meter readings out to 1000 ft showed no detectable change in radiation level.

Integrated doses at 3 ft were measured quite accurately by low-range ionization chambers and pocket ionization chambers with tin sleeves to improve the energy response.

Figures 4.1 and 4.2 show the area used for measurements at a flat dry-lake bed. The ground was hard and smooth with small cracks every few inches.

Figures 4.3 and 4.4 show the plowed field used for measurements. Figure 4.5 contains sketches of the collimator location in relation to the size of the field and shows the approximate size of the furrows and ridges. The furrows ran north and south, and the collimator pointed west.

On the evening of D + 5 day, measurements were made in the center of the fallout path about 8 miles from GZ over typical rough desert terrain. All instrumentation functioned properly, and good data were taken. These data included: (1) energy and angular distribution, (2) dose rate as a function of height (1 to 40 ft), (3) dose rate at 3 ft, and (4) dose rate vs. time (decay). Again there were no detectable changes in the dose rate within 1000 ft of the experimental setup.

Figures 4.6 to 4.8 are photographs of typical terrain at the measurement location.

Several profile surveys were made with a transit to determine the location of washes and ridges in the vicinity of the measurement area. Figure 4.9 is a graph showing the slope of the

ground and the terrain features in the direction the collimator was pointing.*

For correlation purposes, it is hoped that for the final report data concerning the distribution of contamination, decay rates, and spectrum changes with time can be obtained from other groups (Naval Radiological Defense Laboratory or University of California at Los Angeles).

*Since the surface was not horizontal at this location, the data have been corrected for the 2° slope.

Fig. 4.1—Experimental area at a flat dry-lake bed.

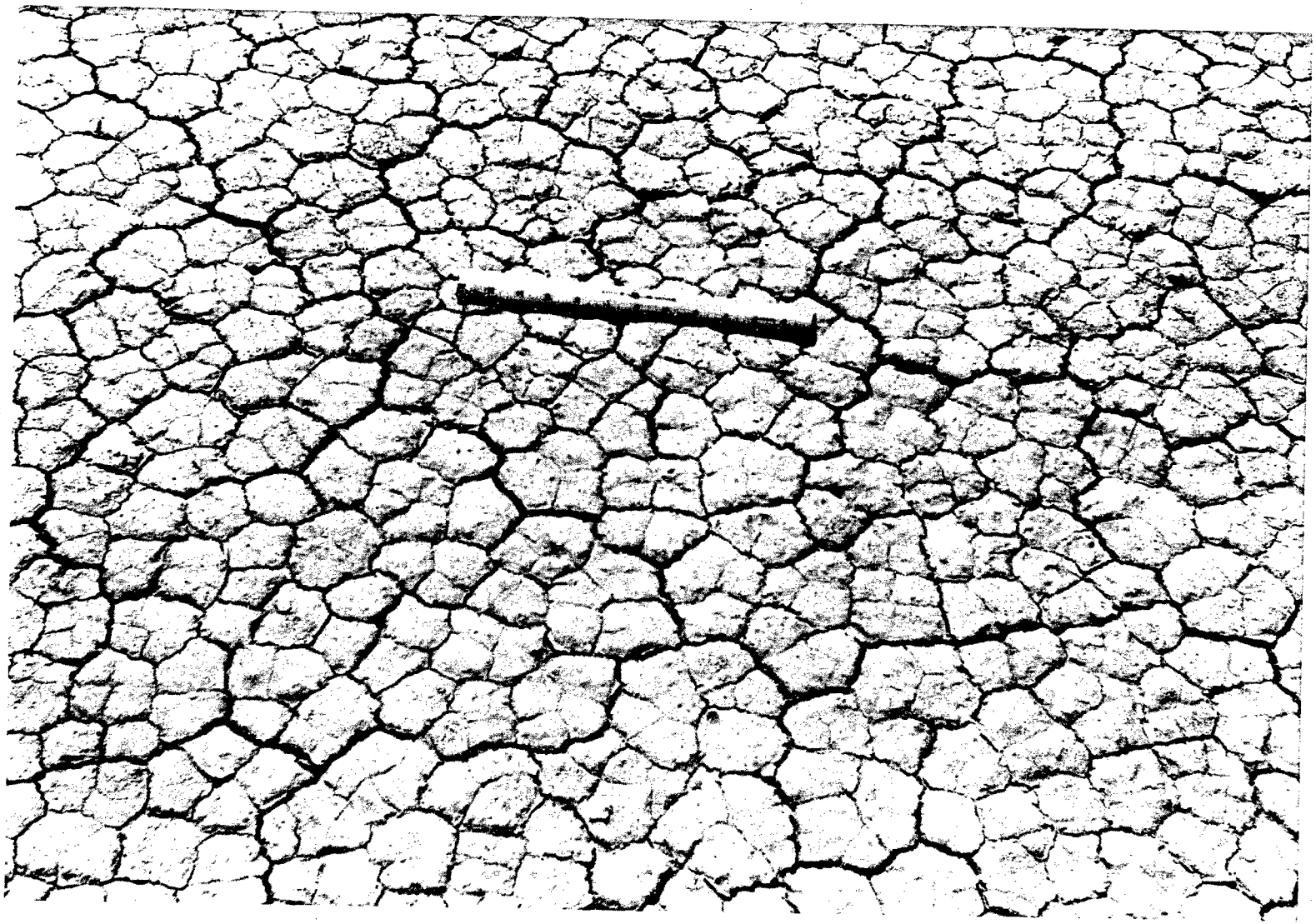

Fig. 4.2—Close-up view of dry-lake bed.

Fig. 4.3—Plowed field used for measurements.

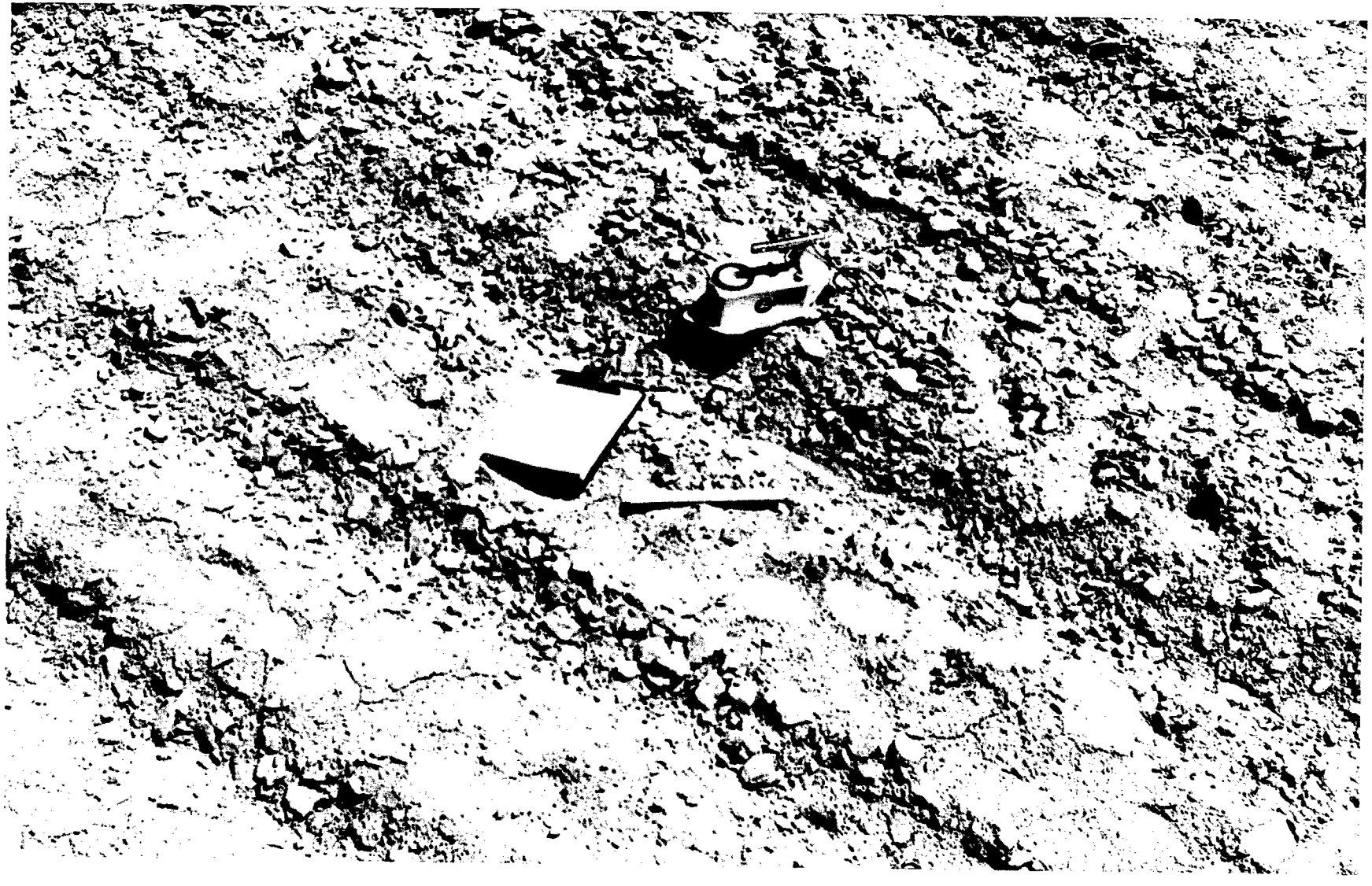

Fig. 4.4—Close-up view of plowed field.

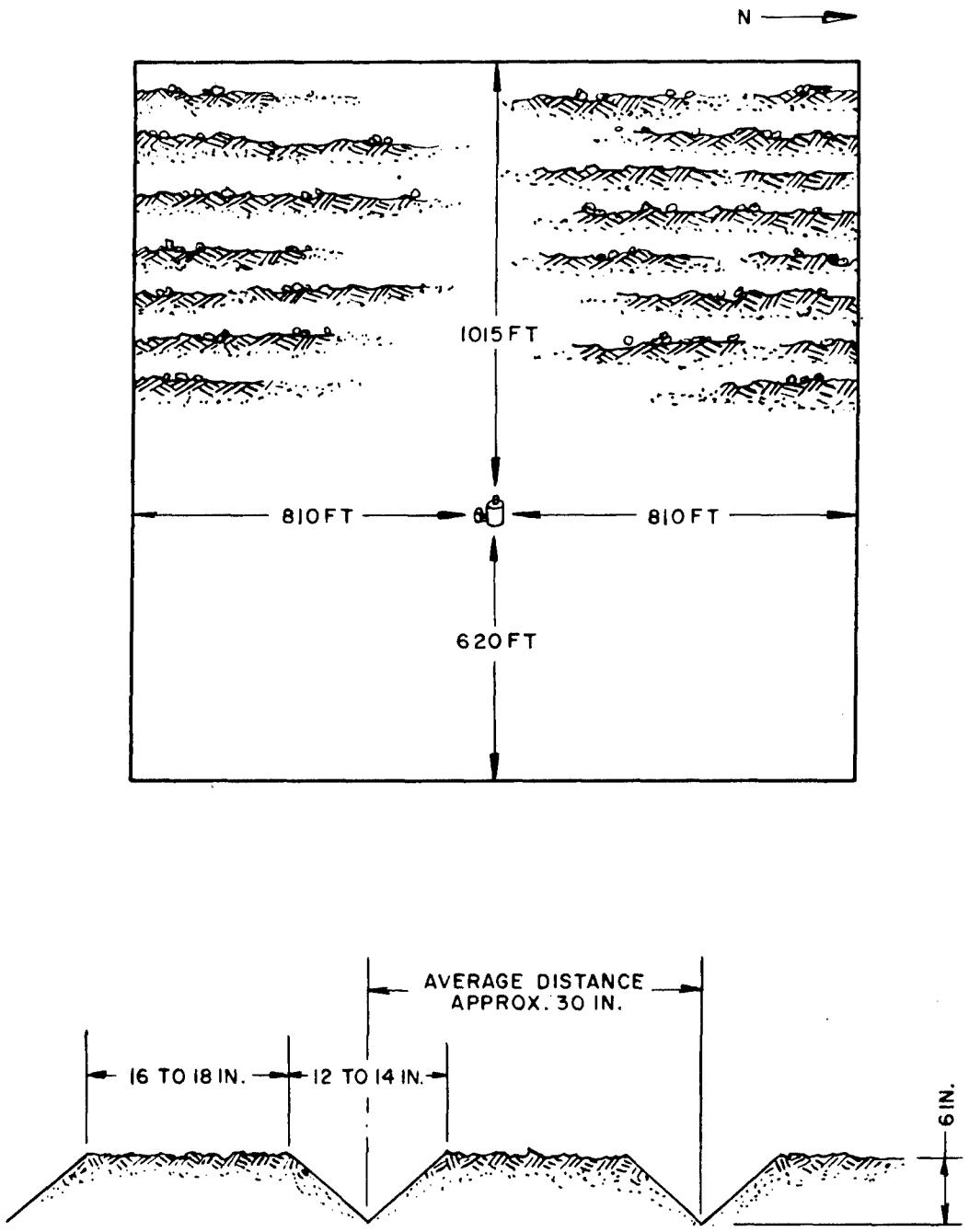

Fig. 4.5—Profile of ground surface, plowed field.

Fig. 4.6—Typical desert terrain.

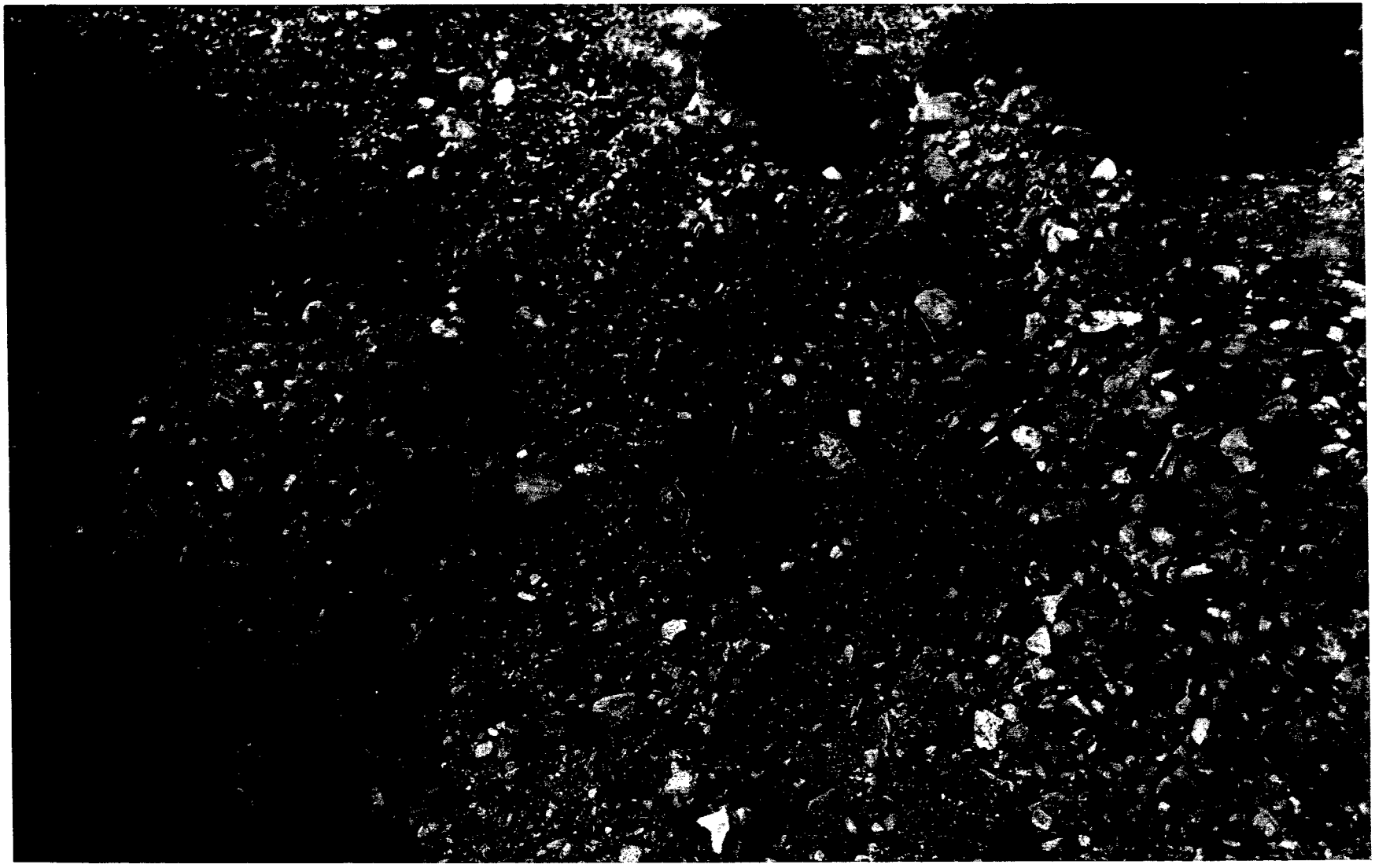

Fig. 4.7—Brush and rocks in desert terrain.

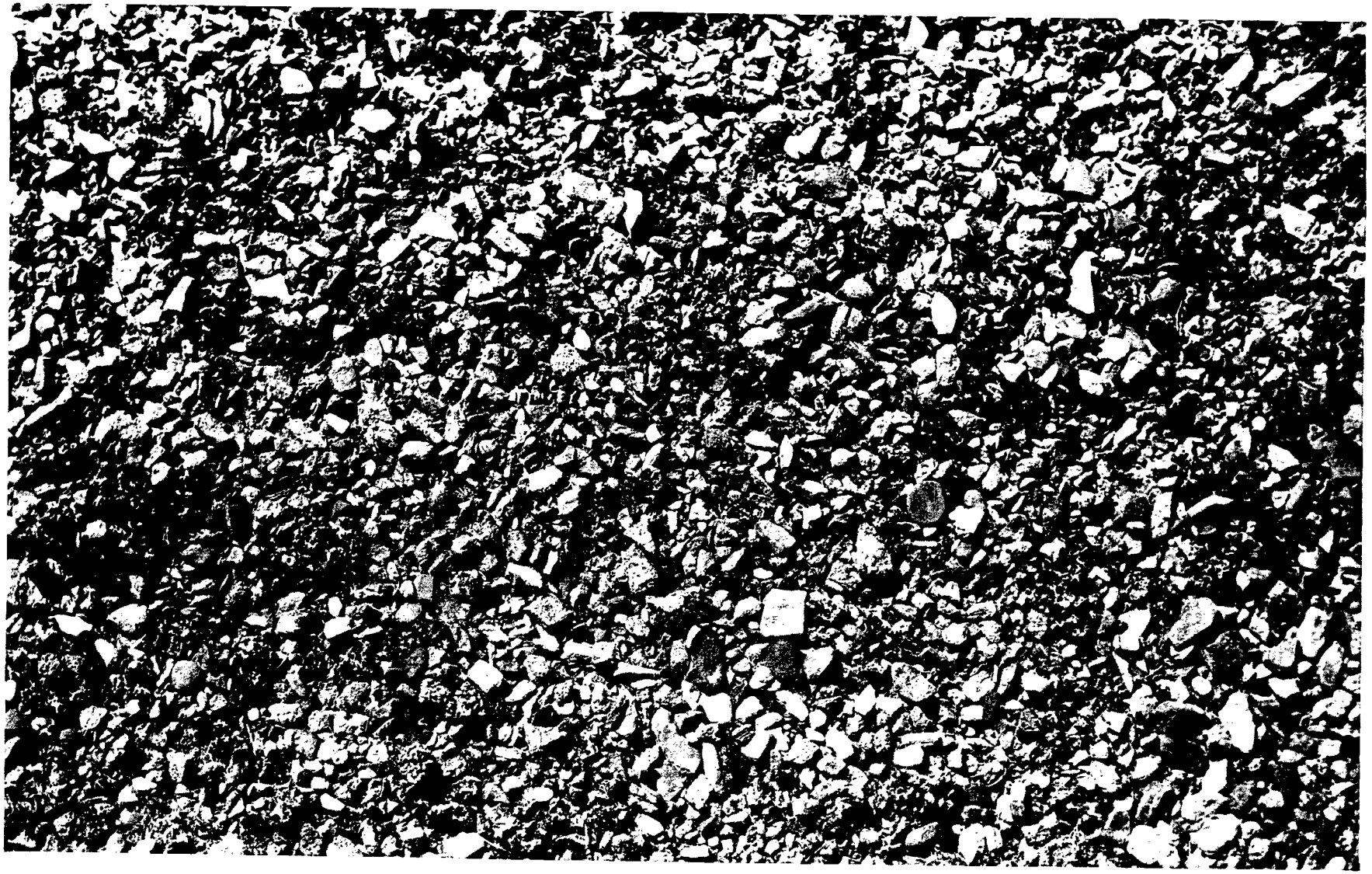

Fig. 4.8—Close-up view of desert terrain. Area shown is roughly 4 sq ft.

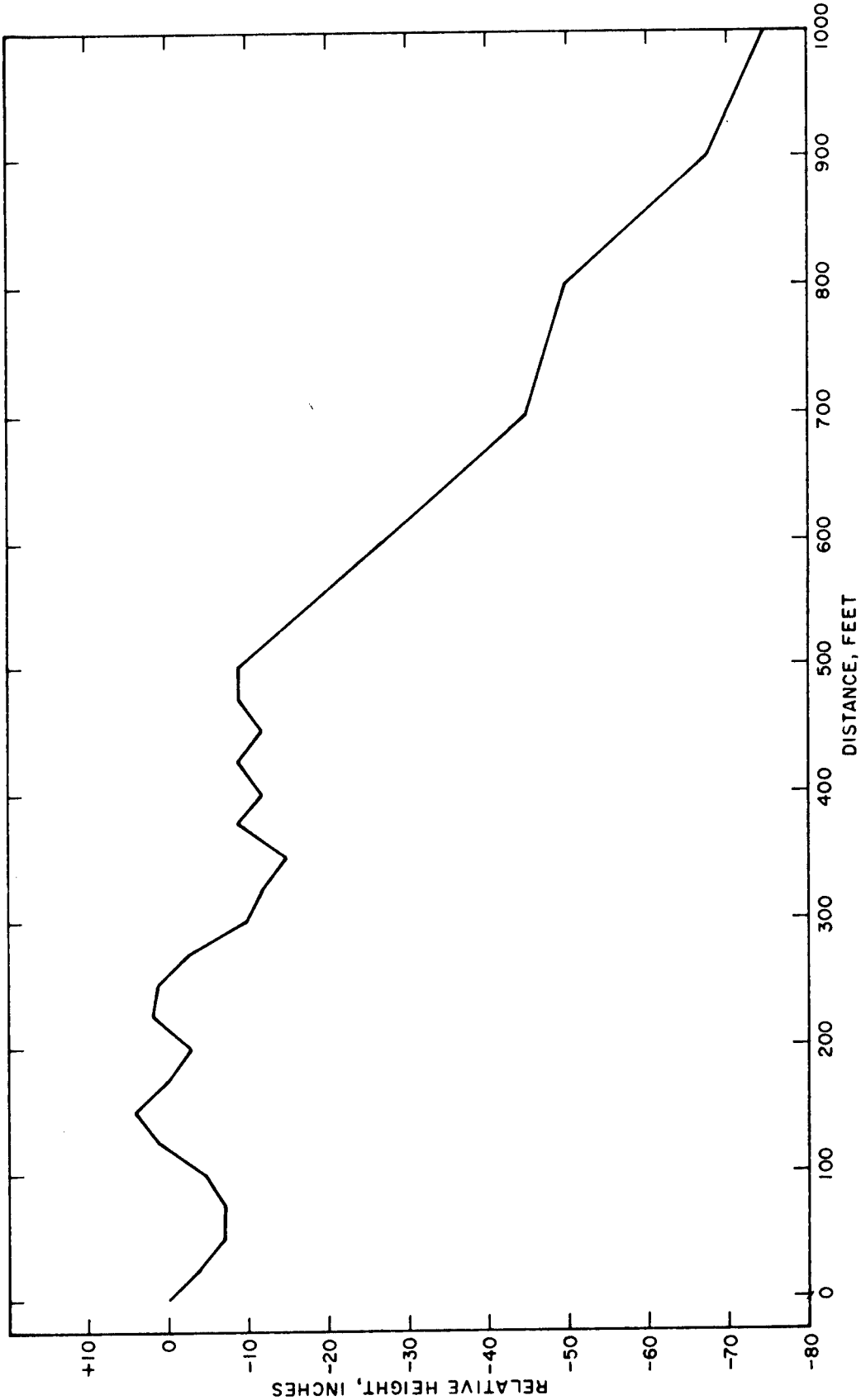

Fig. 4.9—Profile of terrain in the plane of the collimator.

Chapter 5

RESULTS

5.1 DOSE-VS.-HEIGHT MEASUREMENTS

The dose-vs.-height measurements over the dry-lake bed and over the plowed field were not successful because of instrument instability. The dose-vs.-height measurements over the typical desert terrain, however, appeared to be valid. These measurements were made with a Nuclear-Chicago Corporation cutie pie dose-integrating chamber. Doses were measured at heights of 1, 2, 3, 4, 5, 7, 10, 15, 20, 25, 30, 35, and 38.5 ft. Two sets of measurements were made, and the agreement between runs was very good.

The experimental points for dose measurement above the site of the typical desert terrain are shown in Fig. 5.1. The solid curve is a normalized plot of $L(d + \tau)$ for $(d + \tau) = 40$ ft, as described in Sec. 2.4. It is seen that the shape of the curve for $(d + \tau) = 40$ ft is in reasonable agreement with the measurements. It was unfortunate that no comparable data were obtained over the dry-lake bed and over the plowed field.

It should be noted that Fig. 5.1 shows the data points taken approximately 135 hr after detonation whereas the theoretical dose-vs.-height curve applies only for the fallout spectrum 1 hr after detonation.

5.2 DETERMINATION OF DOSE FROM GAMMA-RAY-SPECTRUM MEASUREMENTS

Before the variation of dose with angle can be determined accurately, it is necessary to unscramble the gamma-ray spectra and to compensate for gain shift. Such a detailed analysis will be performed when time permits. In the meantime, however, it is considered advisable to publish tentative results giving estimates of dose at the various angles at which measurements were made.

Approximate results were obtained by using the technique devised by L. Bobisud* while he was working at EG&G (Appendix B).

The results of the calculation of dose (by the method of Bobisud) as a function of angle over the three different types of Nevada terrain are shown in Figs. 5.2 to 5.4.

The data points of Fig. 5.2 show dose plotted against the cosine of the polar angle. For comparison, the theoretical curve of Spencer[1] for a height of 33 ft is plotted as a solid line on the same graph. In interpreting these plots, remember that at least three factors tend to make agreement between theory and experimental data unlikely: (1) the theoretical curve is valid for a 1-hr spectrum whereas the data were actually taken at approximately H + 24 hr; (2) the Bobisud method of computing dose is an approximation that certainly contains inaccuracies; and (3), there were cracks in the dry-lake bed which may have tended to trap fallout particles, as can be seen in Figs. 4.1 and 4.2. If such a trapping effect is important, part of the radiation

*Presently at Los Alamos Scientific Laboratory.

source will be on the surface of the lake bed, and part of the radiation source will be below the surface of the lake bed.

The angular distribution of dose in the case of the plowed ground is shown in Fig. 5.3. (Note the photographs of the plowed field in Figs. 4.3 and 4.4 and the sketch of the transverse profile of the plowed surface in Fig. 4.5.) In this case the usual approximation may not be valid because there was a combination here of two effects: a flat-surface source (between the furrows) and a source that was effectively buried (in the furrows).

Because of the low level of activity in the two preceding cases, any stray activity (either airborne or deposited on the polyethylene sheeting in front of the collimator) would distort the results of the measurements.

In Fig. 5.4 the rough-ground data are presented together with the theoretical curve for an effective height of 33 ft. In this case agreement seems to be good, although, because of the approximations used, this agreement may be fortuitous.

Figure 5.5 shows a comparison between the results of the present investigation and the results obtained by Mather[2] under similar conditions.

Long exposures were necessary to obtain valid statistical data at all three locations. The total number of counts in the worst case (plowed ground, looking toward the zenith) was approximately two and one-half times background. In the most favorable case (looking just below the horizon of the rough terrain), the total number of counts was approximately 50 times background. The other spectra ranged between these limits.

Over all three types of terrain, it is seen that the angular distribution of dose shows a maximum where cos θ is between 0.05 and 0.10. According to the theory developed in Sec. 2.3, this implies that the equivalent height is 0.05 to 0.10 mean free paths. Taking 500 ft as the effective mean free path in air, one obtains τ equal to 25 to 50 ft.

This result is in fair agreement with the conclusions previously drawn from Figs. 5.2 to 5.4.

REFERENCES

1. L. V. Spencer, Structure Shielding Against Fallout Radiation from Nuclear Weapons, *Natl. Bur. Std. (U. S.) Monograph, No. 42* (1962).
2. R. L. Mather, R. F. Johnson, F. M. Tomnovec, and C. S. Cook, *Gamma Radiation Field Above Fallout Contaminated Ground*, Operation Teapot Report, WT-1225, U. S. Naval Radiological Defense Laboratory, Oct. 28, 1959.

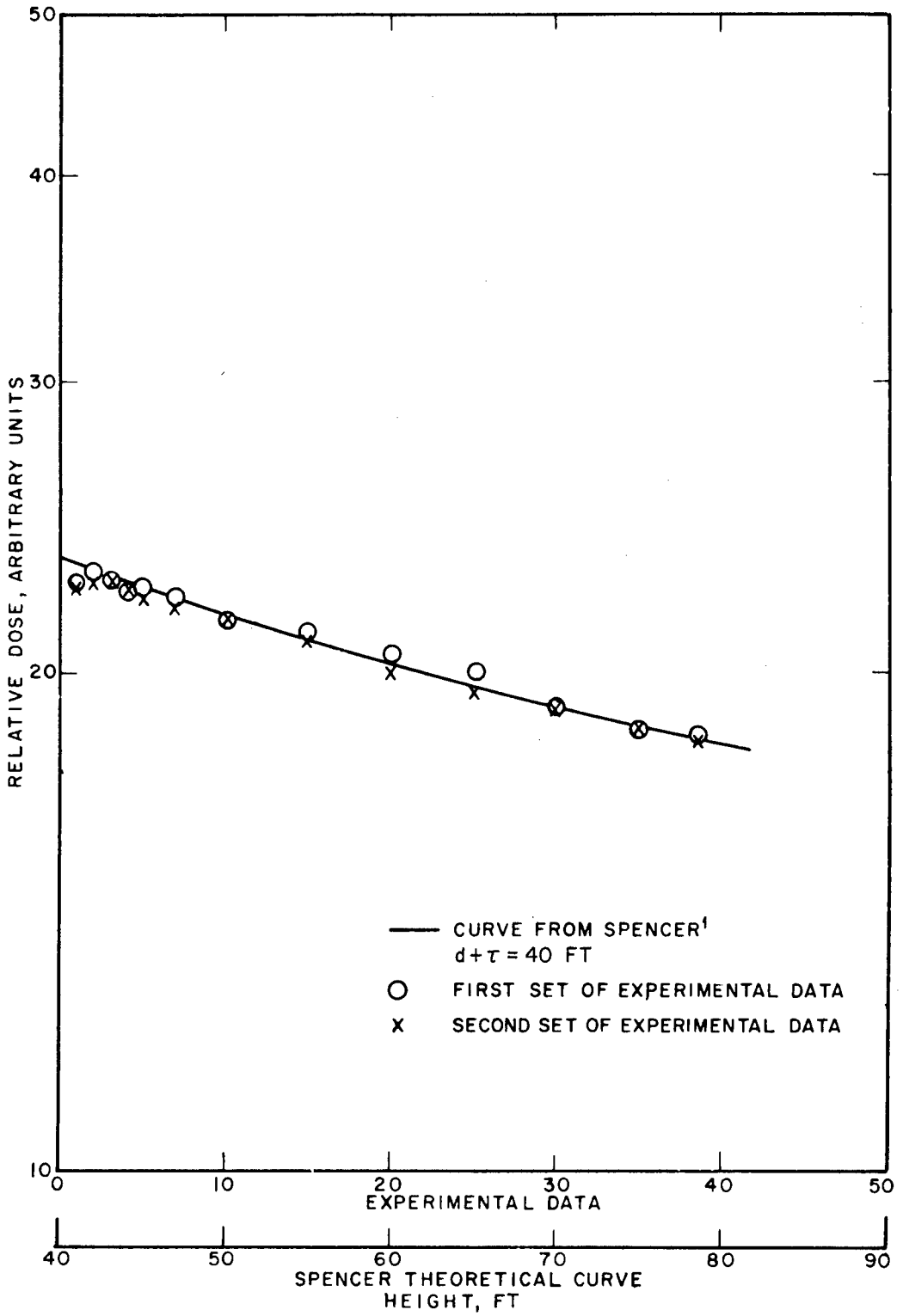

Fig. 5.1—Dose vs. height above typical desert terrain.

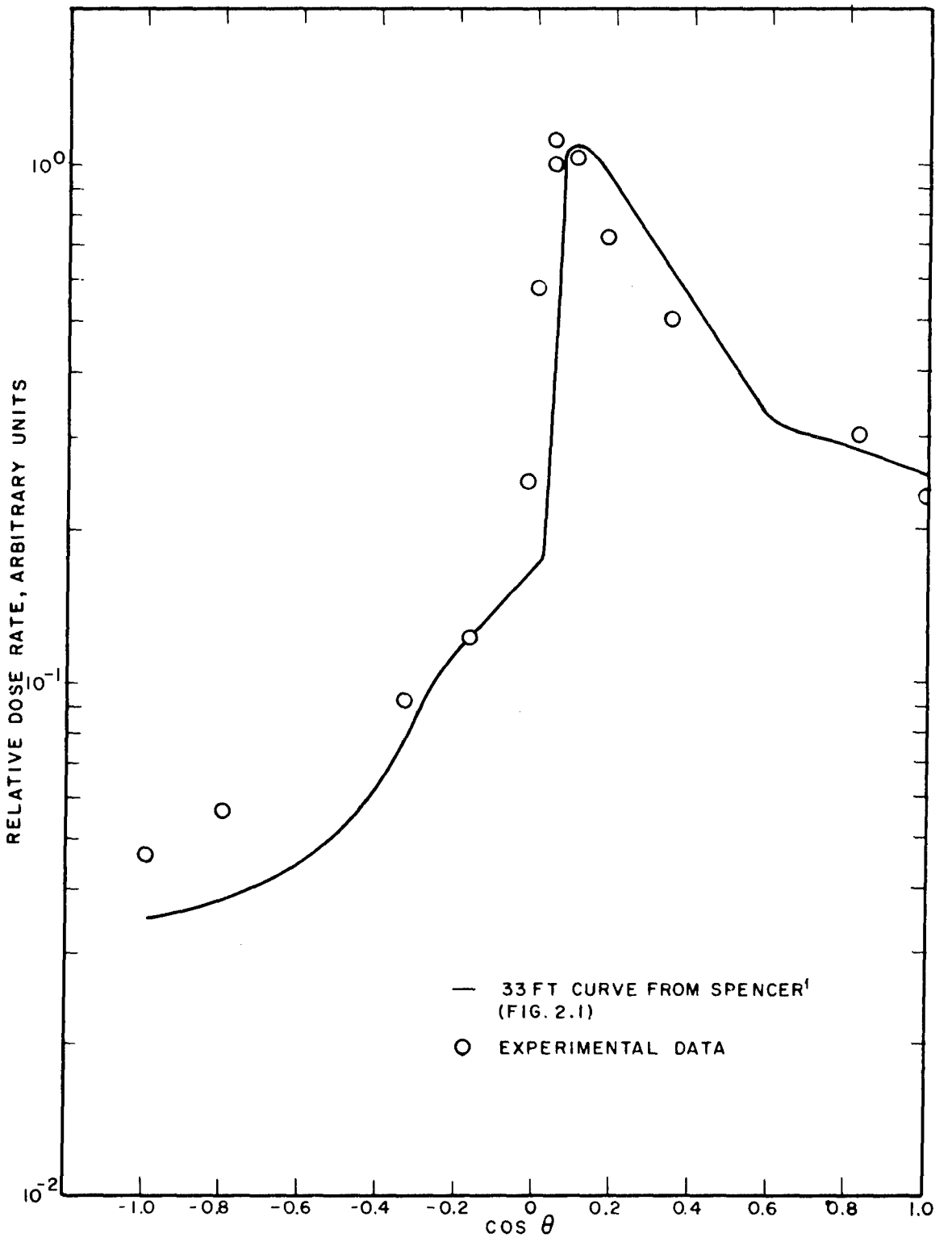

Fig. 5.2—Angular dose above a dry-lake bed.

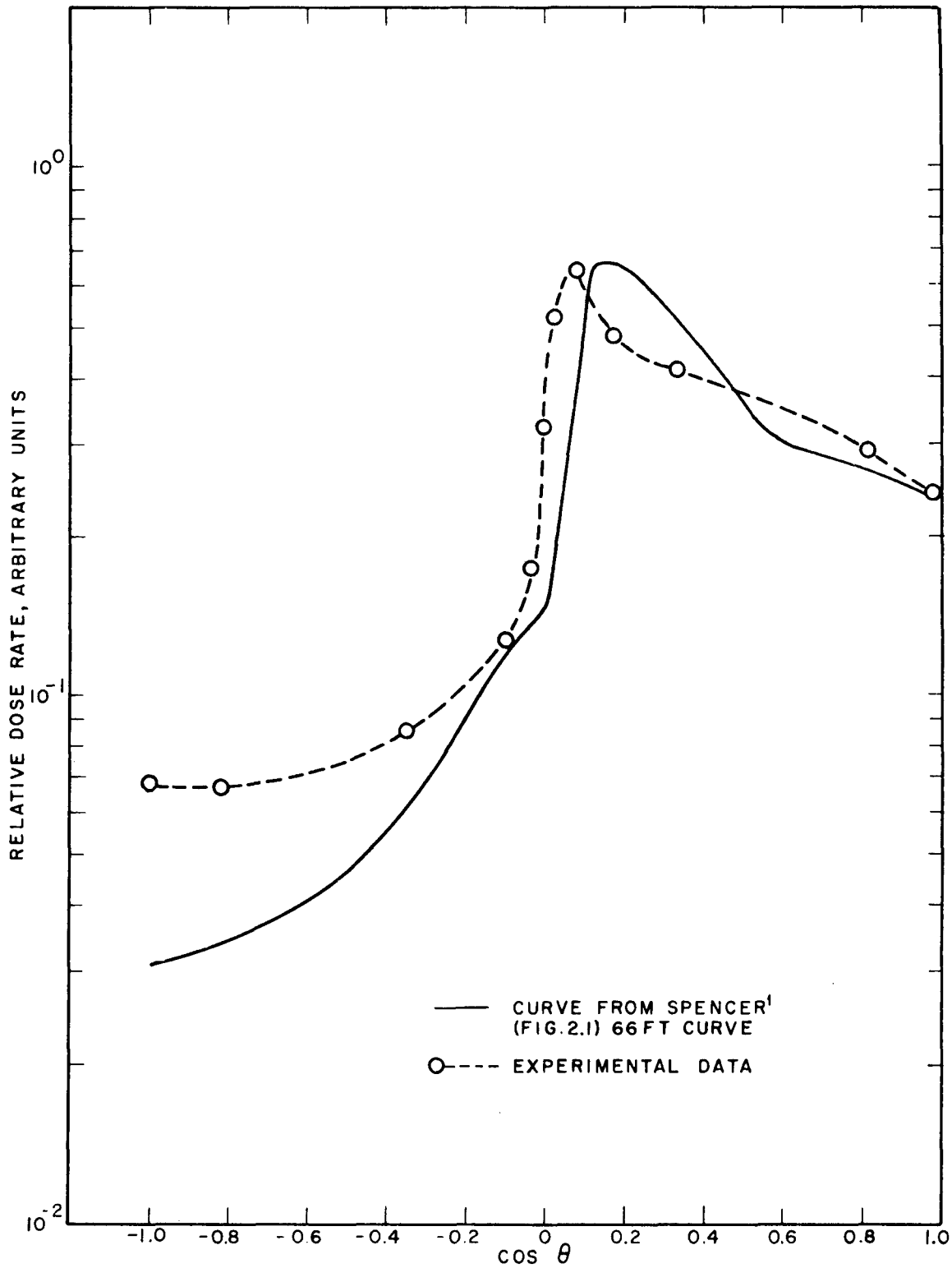

Fig. 5.3—Angular dose above a plowed field.

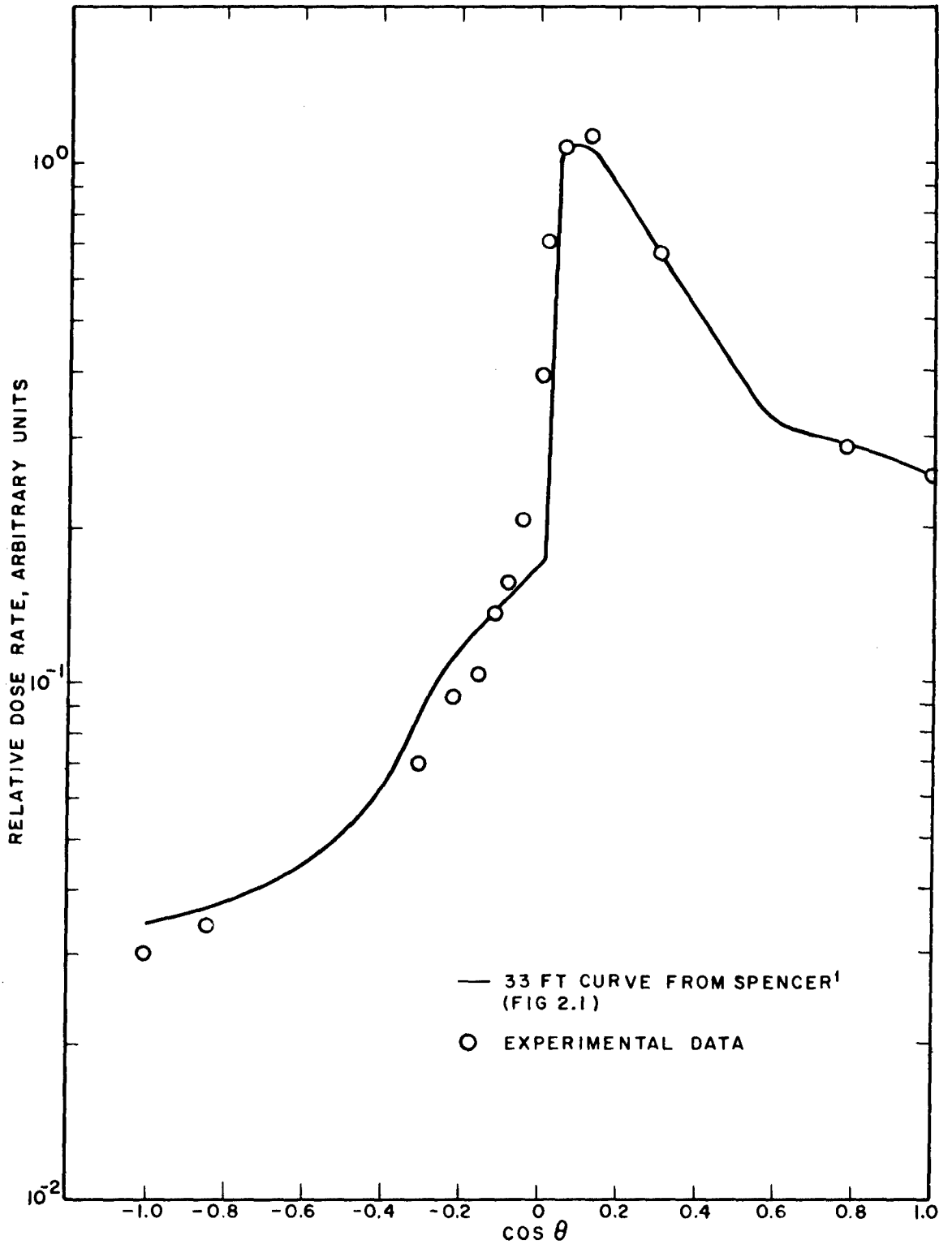

Fig. 5.4—Angular dose above rough desert terrain.

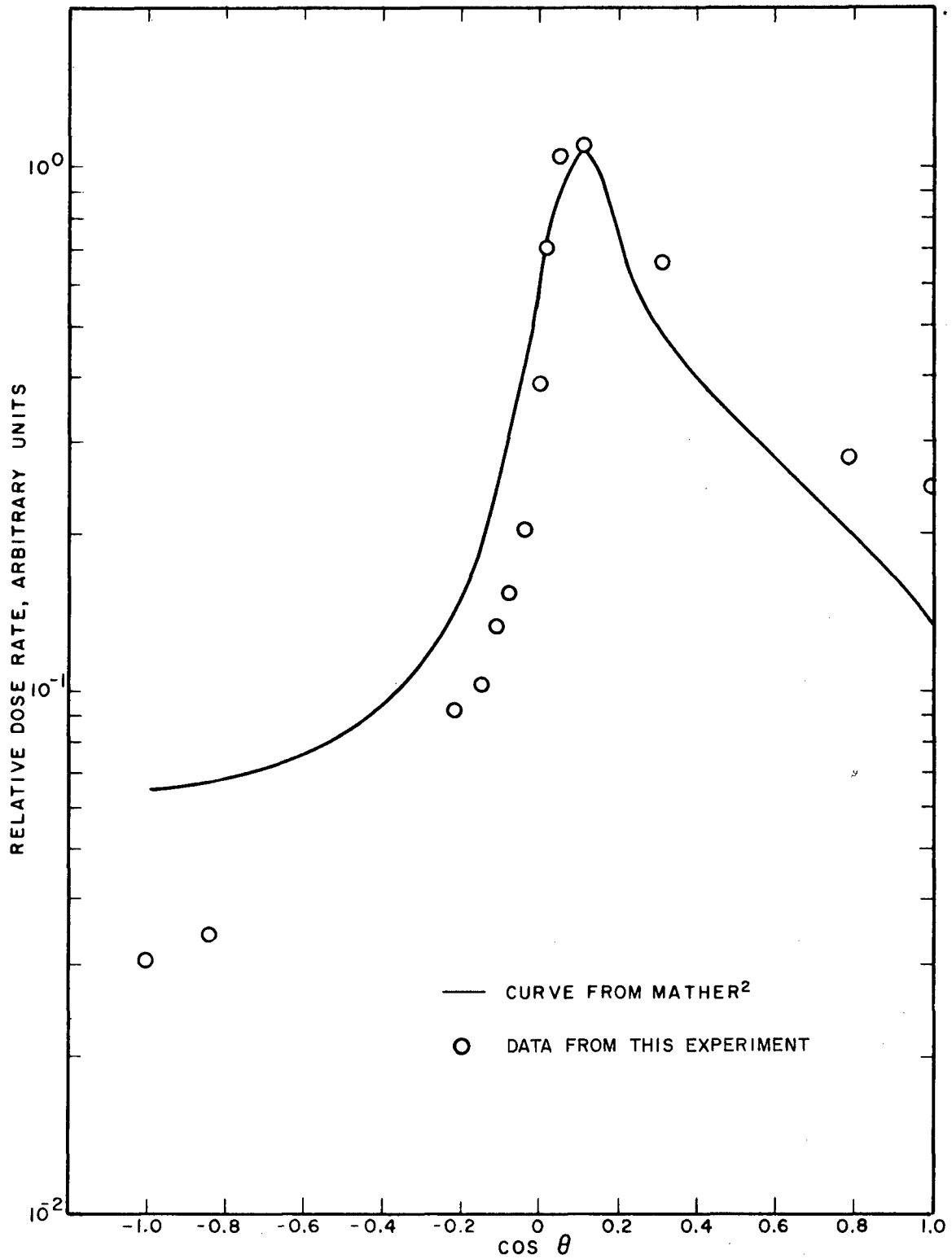

Fig. 5.5—Angular dose above rough desert terrain.

Appendix A

PREDICTION OF FALLOUT CONTOURS

For the experimenters to be prepared in advance, it was necessary to make some predictions concerning probable dose rates to be expected from fallout. It was expected that the experimental equipment would have its best operating characteristics in the 10 to 100 mr/hr range. Therefore it was desirable to know in advance where such radiation fields were likely to occur and to explore the probable regions to become thoroughly familiar with them.

The Effects of Nuclear Weapons (1957 edition) was used as a reference for fallout-pattern predictions.

Fallout patterns can be described in terms of: (1) infinity dose, (2) 1-hr reference dose rate, or (3) the dose rate at time t after the detonation.

Infinity dose at a given position means the total dose accumulated by an observer at the given position from 1 min after detonation until the radiation from fallout has decayed to zero. The value of the infinity dose, computed from 1 min after detonation, is numerically equal to 11.3 times the 1-hr reference dose rate (in roentgens per hour). The infinity dose is expressed in roentgens.

The 1-hr reference dose rate at a given position is the actual dose rate at that position in roentgens per hour. It should be noted that 1-hr reference dose rates are used even at distances greater than the distance travelled in 1 hr by the assumed 15-mph wind. Actually, fallout at the distances being discussed here will not be complete for several hours. The 1-hr reference dose rate is, however, a useful fiction. In all cases the dose and dose rate under discussion are at an elevation of 3 ft above the ground.

The dose rate D_t at a time t hours after detonation is related to the 1-hr reference dose rate D_1 by the formula

$$D = D_1 t^{-1.2} \tag{A.1}$$

From Eq. A.1 and the proportionality between D_∞ and the 1-hr reference dose rate mentioned above,

$$D_t = \frac{D_\infty}{11.3} t^{-1.2} \tag{A.2}$$

At a time 24 hr after detonation,

$$T^{-1.2} = 24^{-1.2} = 0.0218$$

Therefore the dose rate D_{24} 24 hr after detonation is

$$D_{24} = \frac{D_\infty}{11.3} \times 0.0218 = 0.00193\ D_\infty$$

Table A.1 shows approximate residual-radiation 1-hr reference dose-rate contours on the ground for a 1-kt surface burst when the wind velocity is 15 mph.

Table A.1 — RESIDUAL-RADIATION CONTOURS

Dose rate, r/hr	Radius of GZ circle, miles	Displacement of center of GZ circle, miles	Downwind distance, miles	Crosswind distance, miles
1100	0.0368	0.0294	0.368	0.110
368	0.0828	0.0515	0.845	0.257
110	0.1510	0.0828	1.95	0.442
36.8	0.2425	0.1030	4.23	0.662
11	0.349	0.1323	8.28	0.1030
3.68	0.515	0.1543	18.39	0.1875

The displacement of the center of the GZ circle is the distance downwind from the actual to the effective GZ position for purposes of drawing concentric circles of radiation contours. The downwind and crosswind distances are the major and minor axes of an ellipse whose perimeter touches the actual GZ and whose major axis is oriented downwind from GZ.

An approximate scaling law can be given for surface bursts:

$$R = R_0 \times W^{1/3} \text{ at a distance } d = d_0 \times W^{1/3} \tag{A.3}$$

where W is the fission yield of the weapon and R_0 is the 1-hr reference dose rate at a distance d_0 from GZ. This scaling law applies to any of the contour dimensions of the fallout pattern.

From the scaling law of Eq. A.3 and the data of Table A.1, dose-rate contours can be computed for other yields.

As an example, the downwind distance from a 1-kt surface burst is computed for a radiation field of 100 mr/hr 24 hr after detonation when the wind velocity is 15 mph. The answer is found to be approximately 15 miles. For a 2-kt weapon the distance increases to approximately 25 miles.

Doubling the downwind distance results in reducing the downwind dose rate by a factor of approximately 3. Thus, for the case of a 1-kt burst, the 30 mr/hr dose rate after 24 hr would be about 30 miles; for 2-kt the corresponding distance would be 50 miles.

If the wind velocity is different from 15 mph, the distance from GZ for a given radiation contour in the downwind direction is approximately equal to the downwind distance for a 15-mph wind multiplied by the ratio of 15 to the actual wind velocity in miles per hour. It must be realized, however, that this approximation is very crude except for distances greater than 100 miles downwind.

From the foregoing considerations it is apparent that areas out to several miles in the expected downwind direction had to be explored in advance so that the experimenters would be familiar with the territory.

Appendix B

METHOD FOR DETERMINING APPROXIMATE DOSE FROM SPECTRUM MEASUREMENTS

A method is described by which approximate gamma-ray dose rate from spectrum measurements can be obtained without actually unscrambling the spectrum. This method will allow direct calculation of dose from numbers of counts per channel.

Seven channels, 0.275 Mev wide, extending from 0 to 1.925 Mev were used. It is necessary (by the method used here) to have the NaI spectrum of a known monoenergetic gamma ray lying in each channel. This division has the advantage of putting the two Co^{60} peaks of 1.17 and 1.33 Mev in the same channel, that channel extending from 1.100 to 1.375 Mev.

As a first step, the number of counts per second that should be in each channel must be determined. This number will not, in general, equal the number of counts per second actually recorded (see Figs. B.1 and B.2) because various effects, chiefly the Compton effect, in the crystal itself create counts in the lower channels. However, the ratio of counts in a certain channel, say 5, to the counts in a higher channel, say 1, when gamma rays belonging to channel 1 only are present can be determined theoretically from consideration of these effects, or, more readily, from actual NaI spectra. (Actually, since a collimator was used in the experiment, one should be used in determining the various gamma-ray spectra employed. However, the small inaccuracy introduced by using the spectra presented by R. L. Heath in *Scintillation Spectrometry Gamma-Ray Spectrum Catalogue*, USAEC Report IDO-16408, July 1, 1957, is considered tolerable in this application.) In this latter approach the NaI-interpreted spectrum of a monoenergetic gamma-ray emitter having its single gamma ray well within channel 1, such as $_{13}Al^{28}$ with its 1.78-Mev gamma ray, is considered, and the total number B_j of counts in each channel j determined.

Define the constants C_j^i as

$$C_j^i = \frac{B_j'}{B_i'} \qquad i < j$$

where B_j' is the total number of counts in the j*th* channel for B_i' counts recorded in the i*th* channel when the source is known to emit gamma rays falling in the i*th* channel only. Clearly $C_j^i = 0$ if $i > j$.

The accompanying table gives the values of the C_j^i so determined for the range under consideration.

$C_2^1 = 0.47$	$C_3^1 = 0.55$	$C_4^1 = 0.41$	$C_5^1 = 0.41$	$C_6^1 = 0.44$	$C_7^1 = 0.75$
	$C_3^2 = 0.47$	$C_4^2 = 0.50$	$C_5^2 = 0.52$	$C_6^2 = 0.54$	$C_7^2 = 0.62$
		$C_4^3 = 0.51$	$C_5^3 = 0.43$	$C_6^3 = 0.42$	$C_7^3 = 0.47$
			$C_5^4 = 0.44$	$C_6^4 = 0.53$	$C_7^4 = 0.57$
				$C_6^4 = 0.54$	$C_7^5 = 0.70$
					$C_7^6 = 0.45$
	$C_3^{2*} = 0.67$	$C_4^{2*} = 0.72$	$C_5^{2*} = 0.74$	$C_6^{2*} = 0.77$	$C_7^{2*} = 0.88$

The following spectra from the report by Heath (USAEC Report IDO-16408) were used in determining the constants:

1.925–1.650	i–1:	13-28-1
1.650–1.375	i–2:	23-52-1, 59-142-1
1.375–1.100	i–3:	18-42-1
1.100–0.825	i–4:	25-54-3, 12-27-1
0.825–0.550	i–5:	55-137-4
0.550–0.275	i–6:	30-69-1, 4-7-1
0.275–0.00		

The presence of two peaks (0.84 and 1.01 Mev) in the same channel in the case of Mg^{27} was considered inconsequential.*

Defining the C_i^i as

$$C_i^i = Me_i\,(p/t)_i$$

where M is some experimentally determined constant dependent on the source–detector geometry used in evaluating the e_i, which are proportional to the crystal efficiency† for a given source–detector geometry and energy, and $(p/t)_i$ is the peak-to-total ratio for that energy, it is clear that

$$C_i^i = B_i'/A_i' \qquad B_i' = \text{NaI spectra and } A_i' = \text{incident spectra}$$

the primes refer to a monochromatic incident ray (Fig. B.2). Values of C_i^i are as follows:

i	E_i	e_i	$\left(\frac{p}{t}\right)_i$	C_i^i	$\frac{1}{C_i^i(-K_i^i)}$
1	1.788	1.85	0.285	0.53M	1.89/M
2	1.513	1.93	0.315	0.61M	1.64/M
3	1.238	2.03	0.37	0.75M	1.33/M
4	0.963	2.40	0.43	1.03M	0.97/M
5	0.688	2.47	0.53	1.31M	0.76/M
6	0.413	2.96	0.73	2.16M	0.46/M
7	0.138	3.85	0.96	3.70M	0.27/M

*Considerable difficulty was experienced in evaluating the C_j^2 because both gamma-ray peaks used exhibit strong bremsstrahlung in the lower energy channels and neither peak falls in the center of channel 2. Even after the low-energy peaks had been arbitrarily chopped off, it was deemed advisable to multiply the values so obtained (C_j^{2*} of the table) by 0.7, thus reducing the figures to the same order of magnitude as the other C_j^i. It must be admitted that a good deal of human judgment went into determining the values of the C_j^2.

†Stanley H. Vegors, Jr., Louis L. Marsden, and R. L. Heath, *Calculated Efficiencies of Cylindrical Radiation Detectors*, USAEC Report IDO-16370, Phillips Petroleum Co., Sept. 1, 1958. Also presented in R. L. Heath, USAEC Report IDO-16408. The values used are taken from the 40-cm curve for a 3-in. by 3-in.-tall NaI cylinder, times 1000, in the latter reference.

These constants may be interpreted as the recorded counts corresponding to one incident gamma-ray photon.

Having thus determined the C_j^i for all i and j, consider the problem of determining from the number B_i of counts recorded in the *ith* channel the number A_j of counts that should be in the *jth* channel (see Figs. B.1 and B.2). From the preceding equation for the C_i^i (dropping the primes to indicate a continuous incident spectra),

$$A_1 = \frac{B_1}{C_1^1} \tag{B.1}$$

The number of counts b_2 that should be recorded in channel 2 is now equal to the number actually recorded in channel 2 minus the counts recorded in channel 2 from rays properly belonging to channel 1; i.e.,

$$b_2 = B_2 - C_2^1 B_1$$

Dividing this expression by C_2^2, one obtains A_2

$$A_2 = \frac{B_2 - C_2^1 B_1}{C_2^2} \tag{B.2}$$

since $1/C_2^2$ is the ratio of the number of counts actually belonging in channel 2 to the number that should be recorded in channel 2.

Similarly, for the third channel,

$$b_3 = B_3 - C_3^2 b_2 - C_3^1 b_1$$

and

$$\begin{aligned} A_3 &= \frac{B_3 - C_3^2 (B_2 - C_2^1 B_1) - C_3^1 B_1}{C_3^3} \\ &= \frac{B_3 - C_3^2 B_2 - (C_3^1 - C_3^2 C_2^1) B_1}{C_3^3} \end{aligned} \tag{B.3}$$

Anologous equations obtain for channels 4 through 7.

Making an obvious substitution of constants in these seven equations, one obtains

$$A_1 = K_1^1 B_1 \tag{B.1a}$$

$$A_2 = K_2^2 B_2 - K_2^1 B_1 \tag{B.2a}$$

$$A_3 = K_3^3 B_3 - K_3^2 B_2 - K_3^1 B_1 \tag{B.3a}$$

$$A_4 = K_4^4 B_4 - K_4^3 B_3 - K_4^2 B_2 - K_4^1 B_1 \tag{B.4a}$$

$$A_5 = K_5^5 B_5 - K_5^4 B_4 - K_5^3 B_3 - K_5^2 B_2 - K_5^1 B_1 \tag{B.5a}$$

$$A_6 = K_6^6 B_6 - K_6^5 B_5 - K_6^4 B_4 - K_6^3 B_3 - K_6^2 B_2 - K_6^1 B_1 \tag{B.6a}$$

$$A_7 = K_7^7 B_7 - K_7^6 B_6 - K_7^5 B_5 - K_7^4 B_4 - K_7^3 B_3 - K_7^2 B_2 - K_7^1 B_1 \tag{B.7a}$$

The values of the K_j^i thus determined from the C_j^i are

$$K_1^1 = \frac{1.89}{M}$$

$$K_2^1 = \frac{0.77}{M} \qquad K_2^2 = \frac{1.64}{M}$$

$$K_3^1 = \frac{0.44}{M} \qquad K_3^2 = \frac{0.63}{M} \qquad K_3^3 = \frac{1.33}{M}$$

$$K_4^1 = 0.00 \qquad K_4^2 = \frac{0.25}{M} \qquad K_4^3 = \frac{0.49}{M} \qquad K_4^4 = \frac{0.97}{M}$$

$$K_5^1 = \frac{0.02}{M} \qquad K_5^2 = \frac{0.16}{M} \qquad K_5^3 = \frac{0.16}{M} \qquad K_5^4 = \frac{0.33}{M} \qquad K_5^5 = \frac{0.76}{M}$$

$$K_6^1 = \frac{0.01}{M} \qquad K_6^2 = \frac{0.04}{M} \qquad K_6^3 = \frac{0.02}{M} \qquad K_6^4 = \frac{0.13}{M} \qquad K_6^5 = \frac{0.25}{M} \qquad K_6^6 = \frac{0.46}{M}$$

$$K_7^1 = \frac{0.07}{M} \qquad K_7^2 = \frac{0.02}{M} \qquad K_7^3 = 0.00 \qquad K_7^4 = \frac{0.04}{M} \qquad K_7^5 = \frac{0.12}{M} \qquad K_7^6 = \frac{0.12}{M} \qquad K_7^7 = \frac{0.27}{M}$$

The A_i express incident number flux,* and the dose rate D_i in milliroentgens per hour due to gamma rays falling in a given channel i of average† energy E_i is now proportional to the energy flux $I_i(E_i)$ of that channel. The constant of proportionality will be designated Q_i and is tabulated‡ in the following table along with E_i and the product Q_iE_i.

i	$Q_i \times 10^2$	E_i, Mev	Q_iE_i
7	0.17	0.138	2.3×10^{-4}
6	0.20	0.413	8.3
5	0.20	0.688	13.8
4	0.19	0.963	18.3
3	0.18	1.238	22.3
2	0.18	1.513	27.2
1	0.17	1.788	30.4

Thus

$$D_i = Q_i\, I_i(E_i) = Q_i A_i E_i \tag{B.8}$$

where

$$I(E) = E\, N(E)$$

in which N(E) represents the number of particles of energy E.

Substituting into Eq. B.8 the expressions for the A

$$D_1 = Q_1\, E_1\, K_1^1\, B_1$$

$$D_2 = Q_2\, E_2\, K_2^2\, B_2 - Q_2\, E_2\, K_2^1\, B_1$$

$$D_3 = Q_3\, E_3\, K_3^3\, B_3 - Q_3\, E_3\, K_3^2\, B_2 - Q_3\, E_3\, K_3^1\, B_1$$

$$D_4 = Q_4\, E_4\, K_4^4\, B_4 - Q_4\, E_4\, K_4^3\, B_3 - Q_4\, E_4\, K_4^2\, B_2 - Q_4\, E_4\, K_4^1\, B_1 \tag{B.9}$$

*See Chap. 2 of Ref. 1.

†E_i is taken as the central energy of the *ith* channel.

‡Approximated from Table 2.1, p. 17, of Ref. 1.

Now form the following constants

$$Z_1 = Q_1 E_1 K_1^1 - Q_2 E_2 K_2^1 - Q_3 E_3 K_3^1 - Q_4 E_4 K_4^1 - Q_5 E_5 K_5^1 - Q_6 E_6 K_6^1 - Q_7 E_7 K_7^1$$

$$Z_2 = Q_2 E_2 K_2^2 - Q_3 E_3 K_3^2 - Q_4 E_4 K_4^2 - Q_5 E_5 K_5^2 - Q_6 E_6 K_6^2 - Q_7 E_7 K_7^2$$

$$Z_3 = Q_3 E_3 K_3^3 - Q_4 E_4 K_4^3 - Q_5 E_5 K_5^3 - Q_6 E_6 K_6^3 - Q_7 E_7 K_7^3$$

$$Z_4 = Q_4 E_4 K_4^4 - Q_5 E_5 K_5^4 - Q_6 E_6 K_6^4 - Q_7 E_7 K_7^4$$

$$Z_5 = Q_5 E_5 K_5^5 - Q_6 E_6 K_6^5 - Q_7 E_7 K_7^5$$

$$Z_6 = Q_6 E_6 K_6^6 - Q_7 E_7 K_7^6$$

$$Z_7 = Q_7 E_7 K_7^7$$

It is clear that, if D represents the total dose in milliroentgens per hour,

$$\begin{aligned} D &= \textstyle\sum_{i=1}^{7} D_1 \\ &= Z_1 B_1 + Z_2 B_2 + Z_3 B_3 + Z_4 B_4 + Z_5 B_5 + Z_6 B_6 + Z_7 B_7 \\ &= \textstyle\sum_{i=1}^{7} Z_i B_i \end{aligned} \qquad \text{(B.10)}$$

From Eq. B.9 it is apparent that the summation of Eq. B.10 is accomplished by adding the right-hand side of these equations diagonally.

The following values were obtained for Z_i:

$$Z_1 = 26.2 \times 10^{-4}/M$$

$$Z_2 = 23.4 \times 10^{-4}/M$$

$$Z_3 = 18.3 \times 10^{-4}/M$$

$$Z_4 = 12.0 \times 10^{-4}/M$$

$$Z_5 = 8.1 \times 10^{-4}/M$$

$$Z_6 = 3.5 \times 10^{-4}/M$$

$$Z_7 = 0.6 \times 10^{-4}/M$$

If these numbers are now multiplied by the total number of counts in the respective channel and the products are added, the result should be the dose rate in milliroentgens per hour. Making a change of constants,

$$D = \Gamma \textstyle\sum_{i=1}^{7} Z_i^1 B_i$$

where $Z_1^1 = 26.2$

$Z_2^1 = 23.4$

$Z_3^1 = 18.3$

$Z_4^1 = 12.0$

$Z_5^1 = 8.1$

$Z_6^1 = 3.5$

$Z_7^1 = 0.6$

The constant Γ must be determined experimentally.

REFERENCE

1. Herbert Goldstein, *Fundamental Aspects of Reactor Shielding*, Addison-Wesley Publishing Company, Inc., Reading, Mass., 1959.

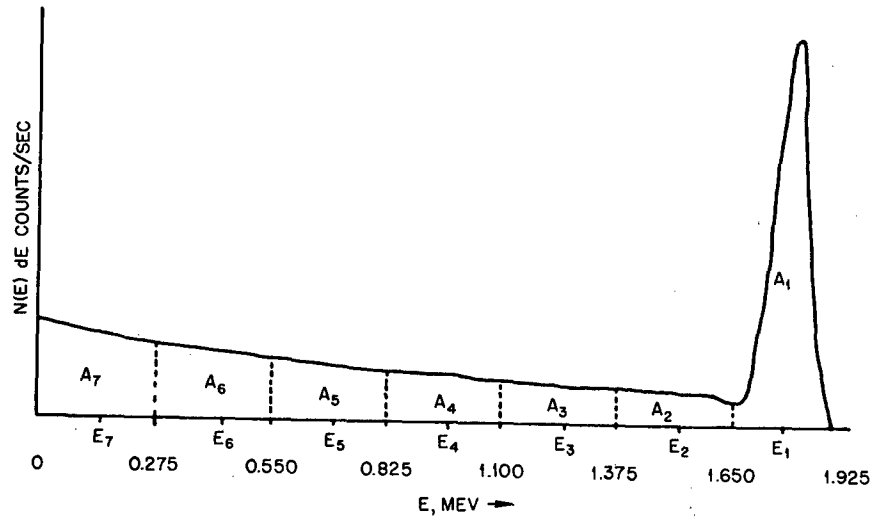

Fig. B.1—Actual, but unknown, gamma-ray spectrum.

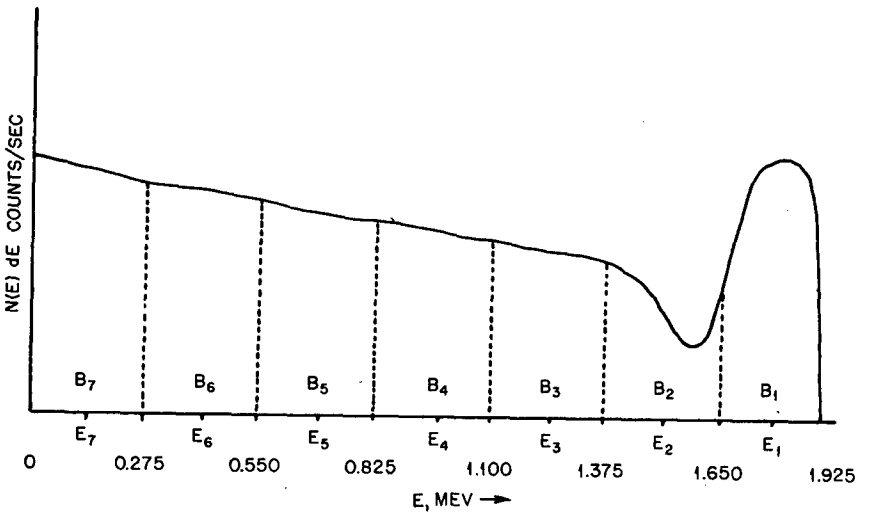

Fig. B.2—NaI-interpreted spectrum.

LEGAL NOTICE

This report was prepared as an account of Government sponsored work. Neither the United States, nor the Commission, nor any person acting on behalf of the Commission:

A. Makes any warranty or representation, expressed or implied, with respect to the accuracy, completeness, or usefulness of the information contained in this report, or that the use of any information, apparatus, method, or process disclosed in this report may not infringe privately owned rights; or

B. Assumes any liabilities with respect to the use of, or for damages resulting from the use of any information, apparatus, method, or process disclosed in this report.

As used in the above, "person acting on behalf of the Commission" includes any employee or contractor of the Commission, or employee of such contractor, to the extent that such employee or contractor of the Commission, or employee of such contractor prepares, disseminates, or provides access to, any information pursuant to his employment or contract with the Commission, or his employment with such contractor.